OULUN YLIOPISTO
UNIVERSITY of OULU

TEKNILLINEN TIEDEKUNTA

AUTOCLAVED DESULFURIZATION SLAG BRICKS - AN OPPORTUNITY FOR CARBON CAPTURE

Markus Honkanen

PROCESS ENGINEERING

Master's thesis

2019

OULUN YLIOPISTO
UNIVERSITY of OULU

TEKNILLINEN TIEDEKUNTA

AUTOCLAVED DESULFURIZATION SLAG BRICKS - AN OPPORTUNITY FOR CARBON CAPTURE

Markus Honkanen

Instructor: Kinnunen Päivö

PROCESS ENGINEERING

Master's thesis

2019

TIIVISTELMÄ
OPINNÄYTETYÖSTÄ Oulun yliopisto Teknillinen tiedekunta

Koulutusohjelma (kandidaatintyö, diplomityö) Prosessitekniikka		Pääaineopintojen ala (lisensiaatintyö)	
Tekijä Honkanen, Markus		Työn ohjaaja yliopistolla Kinnunen Päivö, FT	
Työn nimi Autoclaved Desulfurization Slag Bricks - An Opportunity for Carbon Capture			
Opintosuunta	Työn laji Diplomityö	Aika Heinäkuu 2019	Sivumäärä 57

Tiivistelmä

Tämän diplomityön tavoitteena oli tutkia hiilidioksidin sitouttamista rikinpoistokuonaan ja näin syntyneen materiaalin toimivuutta betonin korvaamisessa rakennusaineena. Työn aikana selvitettiin erilaisten autoklaavi-karbonointiolosuhteiden vaikutusta materiaalin kestävyyteen ja mikrorakenteeseen, sekä haettiin optimaalista hiekan, kuonan ja veden suhdetta mahdollisimman kestävän kuonapohjaisen materiaalin valmistamiseksi.

Työn ensimmäisessä vaiheessa tutkittiin eri hiekan ja kuonan suhteilla valmistettujen näytteiden puristuskestävyyttä lujimman seoksen löytämiseksi. Tulosten perusteella valittiin jatkotutkimuksiin lupaavimmat näytteet, tavoitteena saada mahdollisimman kestävä lopputulos mahdollisimman lyhytkestoisella karbonointireaktiolla ja suurella kuonaosuudella.

Työn toisessa vaiheessa kestävintä seostyyppiä karbonoitiin eri aikamääriä, tarkoituksena testata reaktioajan vaikutusta lopputuotteen kestävyyteen. Karbonoinnin vaikutusta ylipäätään lopputuotteeseen tutkittiin tekemällä kontrollinäytteitä typpipaineistetussa reaktorissa. Myös vaihtoehtoista kuonatyyppiä kokeiltiin raaka-aineena rikinpoistokuonan tilalla. Lopuksi kolmen eri seoksen näytteitä tutkittiin lujuuden lisäksi lämpöstabiiliuden osalta TGA-analyysillä ja kiderakenteen osalta XRD-analyysillä ja elektronimikroskoopilla.

Suoritetun tutkimuksen perusteella saatiin tuotettua näytepaloja, joiden puristuslujuus oli 20 MPa. Puristuslujuus oli noin kymmenen kertaa lujempi, kuin vastaavalla näytteellä ilman hiilidioksidia.

Diplomityö oli osa FLOW-projektia, jossa Oulun yliopiston kuitu- ja partikkelitekniikan tutkimusyksikkö tutkii kiertotalouden ratkaisuja teräksenvalmistuksen sivuvirtojen jatkokäyttöön.

Muita tietoja

ABSTRACT
FOR THESIS

University of Oulu Faculty of Technology

Degree Programme (Bachelor's Thesis, Master's Thesis)	Major Subject (Licentiate Thesis)
Process Engineering	
Author	**Thesis Supervisor**
Honkanen, Markus	Kinnunen Päivö, Dr. (Phil.)

Title of Thesis

Autoclaved Desulfurization Slag Bricks - An Opportunity for Carbon Capture

Major Subject	Type of Thesis	Submission Date	Number of Pages
	Master's thesis	July 2019	57

Abstract

The goal for this thesis was to study the effects of carbon mineralization to the desulfurization slag based mortar and paste samples using autoclave carbonation procedure. During the study, the effects of different carbonation conditions to the compressive strength and crystal structure of a slag brick were tested. Additionally, a number of different mixtures of sand, slag and water were tested to find the most durable and workable composition.

In the first phase of the study, bricks made with different ratios of sand and slag were tested for their compressive strength, in order to find the most durable composition. The results of this phase were used to find the optimal mixture and process conditions to produce as durable bricks as possible with mild reaction conditions and short carbonation time.

In the second phase, the most durable mixture was carbonated for varying time periods to test the effect of the reaction time to the durability of the brick. The effect of the carbonation in general was also tested, by doing control batches of the identical mixtures with nitrogen pressurizing. Another test parameter was the slag type used, for which basic oxygen furnace slag was tested as a substitute for desulfurization slag. After these optimization tests were done, three different mixtures were analyzed using TGA, XRD and SEM imaging for phase composition analysis.

As a result of this study, bricks with compressive strength of over 20 MPa were produced. Samples without carbon dioxide had almost ten times lower compressive strength in otherwise identical conditions.

This master's thesis was part of the FLOW-project. In this project, the fibre and particle engineering research unit of the University of Oulu studies utilization of the by-products of the steel industry.

Additional Information

FOREWORD

The purpose for this work was to examine the effect of carbon mineralization for desulfurization slag's and basic oxygen furnace slag's usability in construction purposes. The work was carried out in the fiber and particle engineering laboratory at the University of Oulu.

I want to express my gratitude to Dr. Päivö Kinnunen for giving me chance to complete my master's studies with this thesis, and for acting as my instructor. I also want to thank the staff of the Faculty of Technology (Dr. Mohammad Mastali, Dr. Juha Ahola, Hoang Nguyen, Elijah Adesanya, He Niu, Jarno Karvonen and Elisa Wirkkala) for helping me conduct my experiments safely and efficiently. Additionally, I was kindly helped with some of my analyses by Pasi Juntunen and Sami Saukko from the Center of Microscopy and Nanotechnology, for which I am really grateful.

Last but definitely not least, I want to thank Dr. Jouni Pursiainen, Dr. Päivi Pirilä and Sonja Immonen for providing me with helpful insight on the writing of this thesis. Their comments and improvement ideas helped me immensely in expressing my thoughts in a systematic manner, thus expediting the writing process and improving the quality of this work.

TABLE OF CONTENTS

ABBREVIATIONS

BOF	Basic Oxygen Furnace
CCU	Carbon Capture and Utilization
C-S-H	Calcium Silicate Hydrate
De-S	Desulfurization Slag
DTG	Derivative Thermogravimetry
E.G.	Exempli Gratia, For Example
FESEM	Field Emission Scanning Electron Microscope
GBFS	Granulated Blast Furnace Slag
SEM	Scanning Electron Microscope
SWEEP	Solid Waste Environmental Excellence Protocol
TGA	Thermal Gravimetric Analysis
XRD	X-Ray Powder Diffraction
XRF	X-Ray Fluorescence

1 INTRODUCTION

As the effects of the global warming become constantly more evident (Vautard et al., 2014), the importance of applying concepts such as circular economy appear to be ever more urgent. The biggest contributors to industrial pollution are metal industry, pulp and paper industry, oil industry and stone quarries (Vallero, 2014), thus giving them the biggest potential to affect global emissions with their actions. One way that the steel industry has tried to apply waste-to-resource supply chain, has been the research for aluminosilicates, more commonly known as slags, as a raw material. In practice this has meant testing the suitability of different slag types in various uses. The slag is produced roughly 10-15% by weight of the produced steel (Proctor et al., 2000), and an estimated crude steel production in 2017 worldwide was 1691.2 Mt (World Steel Association, 2018). This means roughly 200 million tons of slag produced annually. To waste this potentially reusable material in a landfill would be unsustainable from both environmental and economic standpoints. Moreover, according to SWEEP (Solid Waste Environmental Excellence Protocol), the annual growth for the landfill costs have been 2.0% in the US from 2010 to 2016. So apart from causing environmental damage in landfills and loss of revenue in the form of underutilizing a side stream of a process, finding an inexpensive way of storing the slag continues on getting harder.

Another major contributor to climate change apart the steel industry is cement manufacturing. According to Miller et al. (2018), the cement production caused 8% of global carbon dioxide emissions in 2012. The production of cement increased 18% globally from 2012 to 2015, simultaneously increasing the carbon dioxide (CO_2) emissions. Since the demand for cement manufacturing is on the rise, finding alternative ways for production processes is becoming constantly more important in an economic sense. In the cement production, 50% of the carbon dioxide emissions are caused by thermal decomposition of calcium carbonate to lime and carbon dioxide. The rest is produced by the use of energy, especially from the combustion of fossil fuels (Nisbet et al., 2002). This would suggest, that the most effective ways of reducing emissions in the cement production can be found in alternative raw material research and more ecological energy production.

The present study looks into desulfurization slag and basic oxygen furnace slag (BOF) as raw materials for construction purposes. A method, that efficiently produces concrete applicable for construction, and that uses industrial waste as a raw material would be both economically and ecologically interesting. The usage of inorganic cements by valorizing industrial by-products is not a new technology, as there have been experiments with alkali activation for over a century. In past decades this technology has, however, improved enough to yield commercial uses for products such as alkali activated granulated blast furnace slag (GBFS). The current challenge is to seek more slag types apart from GBFS that have enough hydraulic reactivity and low amount of heavy metals to make a suitable building material (Criado et al., 2017).

1.1 Alkali Activation

The alkali activation is a reaction, in which an aluminosilicate, such as desulfurization slag or BOF slag, is mixed with an alkali activator to form a hardened material with good binding properties. The alkali activators are typically alkaline salts or caustic solutions such as sodium silicate or sodium hydroxide. Since these slag materials have high amounts of calcium and silicon, a calcium silicate hydrate (C-S-H) gel can be produced in relatively moderate alkaline conditions (García-Lodeiro et al., 2015).

The C-S-H abbreviation is a cement chemist notation, which is used to simplify the formulas used to describe the compounds found in cement materials. The actual formula for C-S-H varies within the range of 0.6–2.0 $CaO \cdot SiO_2 \cdot 0.9–2.5\ H_2O$, with occational partial substitution of aluminum for silicon (Locher, 2006). Producing C-S-H is important for the cement based material, as it is primarily responsible for its strength capabilities. It is produced as a result of a reaction between water and the silicate phases of the cement material. The reaction is typically expressed in the form shown in Eq. 1 (Kurtis, 2017).

$$2Ca_3SiO_5 + 7H_2O \rightarrow 3CaO \cdot SiO_2 \cdot 4H_2O + 3Ca(OH)_2 + 173.6\ kJ \quad (1)$$

The slag reactivity depends largely on the amount of vitreous phase content, mainly depolymerized calcium silicate, but there have also been good results with slags with lower vitreous contents (30-65%) (Pal et al., 2003). There are some requirements for

slag to be usable in activated cement that are widely accepted in literature (Shi et al., 2006; Provis and van Deventer, 2009). The slag should be granulated or pelletized to a specific surface of 400-600 m^2/kg, and ideally have large vitreous phase content (85-95%). It should have some structural disorder to improve its hydraulic activity due to lower polymerization degree in the vitreous phase. The polymerization degree itself depends on the coordination of SiO_4, aluminum and magnesium in the vitreous phase. The pH of the slag should be basic, as basic slag has higher hydraulic potential than acidic one. The reason for this is the lime content of the basic slag, which controls the activation reaction. However, this does not mean that acidic slag could not be alkali-activated as well.

The basic reaction mechanism for alkaline activation has been modeled by Glukhovsky and Krivenko (Glukhovsky, 1994; Krivenko, 1994) with series of reactions shown in Eq. 2. In the model, the alkaline cation (R^+) is the catalyst in the hydration via cationic exchange with Ca^{2+} ions. The alkaline cation of the catalyst can vary depending on the microstructure wanted on the end product. If e.g. high amount of zeolite formations are wanted, Na^+ should be considered, since it is a small cation with low charge density, and thus able to flow more freely through the gel.

$$\begin{aligned} &SiO^- + R^+ \rightarrow SiOR \\ &SiOR + OH^- \rightarrow SiOROH^- \\ &SiOROH^- + Ca^{2+} \rightarrow SiOCaOH + R^+ \end{aligned} \quad (2)$$

The end product of this reaction path is a calcium silicate hydrate, which occasionally has aluminum in its composition (García-Lodeiro et al., 2015).

1.2 Desulfurization Slag

In steel-making process, iron is extracted from iron ore by reduction with carbon monoxide (Eq. 3), and further refined into steel. In a secondary refining process, a desulfurizer agent consisting of lime and fluorspar is used to treat the liquid iron. This refining causes a layer of slag to form on the liquid iron, from which the sulphur is removed by a slag-liquid metal reaction (Eq. 4) (Chen et al., 2018).

$$Fe_2O_3 + 3CO \rightarrow 2Fe + 3CO_2 \quad (3)$$

$$Ca^{2+}_{(slag)} + S^{2-}_{(iron)} \rightarrow CaS_{(slag)} \quad (4)$$

The desulfurization slag (De-S) has usually been considered to be waste despite its relatively high iron contents, since it also contains sulphur collected from the liquid iron. The sulphur content of the De-S samples used in present study were roughly 2%, compared to 0.07% found in the BOF slag. Thereby the sulphur content of De-S is considerably lower than e.g. its calcium or iron contents, yet much higher than in other slag types.

Desulfurization slag is considered non-toxic, and it contains high amounts of calcium and silicon, which makes it suitable for cement production among other uses. The cement industry has been interested in using different waste materials in their raw material streams in recent years, since the natural supplies for their manufacturing processes have been depleting steadily. Other major factor in this interest has been constantly increasing pressure to address the environmental issues within the cement production. Iron and steel-making industries have had a common interest with these goals, as they produce various kinds of slags, most of which contain large amounts of lime and silica. It is seen as a benefit for both industries, if cement manufacturers can find an environmentally friendly, synthetic raw material from the side streams of iron and steel industries (Chen et al., 2017). All the components found in the De-S, with >1% concentration, are shown in Table 1. The composition was defined using an XRF analysis method. The complete result for the XRF analysis of the De-S can be found in Appendix 1.

Oxide	**CaO**	**Fe_2O_3**	**SiO_2**	**SO_3**	**Al_2O_3**	**MgO**	**Na_2O**
Concentration (%)	55.4	16.1	15.2	5.0	2.2	1.6	1.5

Table 1. Chemical composition of De-S (XRF).

Among the most successful investigations for the reuse of De-S specifically, have been the applications in controlled low-strength concrete (Huang et al., 2016) and heavy metal adsorption (Wu et al., 2014). In the research done by Huang et al., De-S was found to improve the workability of the concrete slump (2016). It was also reported to lower the weight of the concrete compared to the one made with natural fine aggregates, though lowering its strength by 36.1 - 62.5% at the same time. That being said, the compressive strength still ended up being within the locally required 9 MPa range after 28 days of drying. The maximal drop value (the height from which the sample can be dropped without fracturing it) was found to increase 25% to 7.6 cm when 50% replacement was employed, making the concrete sufficient for continuous construction and loading support by Taiwanese regulations. Huang's research also found the ultrasonic pulse velocity and surface electric resistance to decrease, though the erosion and swelling increased as well up to the point of failure at the replacement portions above 50%. As a summary, Huang et al. suggests, that moderate replacement of natural fine aggregates with De-S would reduce construction time and enable lighter structures with low-strength concretes (2016). In Figure 1, the appearance of the desulfurization slag used in the present study can be examined.

Figure 1. Desulfurization slag mixed with sand and water.

1.3 BOF Slag

Basic oxygen furnace slag (BOF) is glass-like by-product of steel production, mainly consisting of the oxides of calcium, silicon, magnesium, aluminum and iron (Fruehan, 1998). BOF has been traditionally used e.g. as an aggregate in road construction, though the problem with this application is the slag's tendency to expand up to 10% over time, thus deteriorating the roads in longer periods of usage. The volumetric expansion is caused by unhydrated lime (CaO) contained in the slag, reacting with water to produce calcium hydroxide ($Ca(OH)_2$). This expansion can be prevented to certain degree with steel slag aging, combined with testing and quality control, though this increases the costs of using said material (Wang et al., 2010). In the Table 2 the chemical composition of non-carbonated BOF slag can be found for the components with >1% concentration. The complete result for the XRF analysis of the BOF slag can be found in Appendix 2.

Oxide	**CaO**	**Fe_2O_3**	**SiO_2**	**V_2O_5**	**MnO**	**MgO**	**Al_2O_3**
Concentration (%)	50.1	23.4	14.3	3.2	2.9	1.9	1.7

Table 2. Chemical composition of non-carbonated BOF slag (XRF).

In their study, Shu-Yuan et al. suggest that by carbonating the alkaline solid waste from the steel mills, and using it in cement industry reduces the carbon dioxide emissions by roughly one ton per one ton of treated slag (2017). The carbonation might also help with the expansion problem of the slag, making it a potential raw material for construction purposes. The details behind the carbon capture reaction are explained further in chapter 1.4 Carbon Capture and Utilization.

1.4 Carbon Capture and Utilization

The oldest concept of carbon capturing is based on a phenomenon called carbon sequestration, in which carbon dioxide is bound into a chosen reservoir such as soil, bedrock or ocean. In practice this means accelerating the natural weathering of silicate

minerals, to form stable products such as carbonate minerals and silica. These reactions are typically exothermic and thermodynamically favoured (Sedjo and Sohngen, 2012; Lackner, 2003).

The main difference between the carbon capture and utilization (CCU) and carbon sequestration is that in CCU the captured carbon dioxide is reused for conversion into other substances or production of products such as plastic, fuel, or concrete instead of just storing it in bedrock. The goal in CCU technologies is to re-use carbon dioxide in manufacturing process while maintaining carbon neutrality for the entire production (Cuéllar-Franca and Azapagic, 2015).

The current situation with organizations exploring the potential of mineral carbonation include companies such as Greensand, which uses ground olivine products to fertilize land with magnesium deficiency, simultaneously absorbing carbon dioxide from the atmosphere (Schuiling, 2011). Another application has been seen from a Californian cement manufacturer Calera, which produces cement additives from carbon dioxide and calcium received from other processes sidestreams. With flue gas used as a reagent in this process, the total amount of Portland Cement replaced in concrete with calcium carbonate has been 15%.

The research conducted by Cicek and Tanriverdi was a basis of the carbonation experiments in the present study, due to the similar conditions and materials used in their article (2007). One of the interests for the research was to find as economic conditions as possible for the carbon capture by using low temperature and pressure. The carbonation process is challenging to monitor due to the potentially high number of reactions occurring, all of which are dependent on several parameters. For example, if the carbonation is conducted in aqueous conditions, there are six major reaction steps that needs to be taken into consideration. These steps are solvation to the liquid, hydrolysis of carbon dioxide and forming of the carbonic acid, dissociation of the carbonic acid into bicarbonate and carbonate ions, dissolution of the minerals and releasing of the reactive metals into liquid, diffusion of the ions, and precipitation of secondary minerals (Santos and Van Gerven, 2011). There are a limited number of articles about carbonation in the autoclave conditions with the chosen temperature and pressure range. This made the present study a good chance to investigate the

carbonation phenomenon from a different point of view, and to potentially make some new findings in the field.

1.4.1 Affecting Variables

There are several variables that affect any given reaction depending on the complexity of the reaction. To be able to compare two reactions and to make logical conclusions about the results, one must understand which variables affect the observed reactions and how. The experiments performed in the present study have many factors that may affect the outcome of the reactions. To keep the experiments repeatable and the results comparable to similar studies, the factors that affect the outcome of the reactions the most were carefully observed and kept as constant as possible.

The first variable that affects any reaction step is temperature. The higher temperature expedites the mineral dissolution from solid to liquid, but it also reduces carbonate and carbon dioxide solubility. Bauer et al. found, that despite the reducing the carbonate solubility, the higher temperature increases the overall carbon dioxide binding, as well as calcium dissolution and silicate carbonation (Bauer et al., 2011, Polettini et al., 2016).

Another crucial parameter to follow is pressure. According to the Henry's law, carbon dioxide solubility in the liquid increases along with the increased pressure: at 25 ^{o}C the molar fraction of carbon dioxide increases from $6.22 \cdot 10^{-4}$ to $3.01 \cdot 10^{-3}$, when increasing the pressure from 101 kPa to 500 kPa. The increase is even greater at higher temperatures. This correlation has been found to be viable in temperatures from 273 K to 433 K (0 to 160 ^{o}C) (Carroll et al., 1991). Due to this, most of the available research has focused on high pressure and high temperature conditions, despite the costs of trying to implement those conditions to industrial manufacturing scale.

With the solid material (slag and sand), the particle size and porosity affect the carbon dioxide uptake, since they determine the surface area which takes part in the reaction. The finer and more porous the particle is, the larger surface area that is in contact with carbon dioxide is and the greater the dissolution rate of the minerals is (Polettini et al., 2016). For example, Huijgen et al. managed to triple the calcium conversion in their

experiments by changing the particle size of the steel slag from < 2 mm to < 38 μm (2005).

The mineralogical composition of the alkaline material has also been found to affect the carbon dioxide uptake. In the research conducted by Bodor et al., simple oxides and hydroxides of calcium and magnesium showed the greatest carbonation yields, whereas silicates and aluminosilicates displayed only some degree of carbonation depending on their structure and chemical properties (2013). In the same article calcite was found to be preferred alkaline in the phases containing calcium and aragonite for magnesium containing minerals. (Bodor et al., 2013).

The amount of water in the reaction is one factor that affects the carbonation efficiency. It improves hydration, dissolution and diffusion, though excess water may also act as a mass transfer barrier that reduces the carbon dioxide diffusion, along with increasing the heating requirements for the reactor (Baciocchi et al., 2010). In the present study, the moisture content was addressed by saturating the samples with water before pressing the mixture into a mold with 20 MPa, which removed the excess water. The reaction was then executed in dry conditions.

It should be noted, that there are numerous reactions occurring simultaneously during the carbon capture, many of which affect one another. This makes it challenging to reliably assess which parameter affects the total process, since the effect may change when the reactor settings are altered. The reaction parameters that were chosen to be monitored were temperature, pressure, curing time and brick composition (ratio of water, silica sand and slag, pressing force).

1.5 Sample Forming

Steel slag's mineral composition has been found to be similar to the chemical components of cement, thus making it a potential research subject as a construction material. The main issue with using steel slag in concrete has been its tendency to expand in volume, due to free oxides, mainly CaO, MgO, SiO_2 and FeO, found in the slag. The primary reason for expansion is the reaction of CaO with water to produce $Ca(OH)_2$, simultaneously expanding the slag (Montgomery and Wang, 1993). If this

challenge can be overcome, however, the brick production could have a significant effect on lowering production costs and protecting the environment (Peng-Guan and Feng-Qing, 2016).

In the present study, the potential of desulphurization slag and BOF slag for lime brick and carbonation reactions was examined. In the sample forming phase slag, water, and varying portion of silica sand was pressed with 20 MPa pressure to form small bricks. The reason behind this step was to consolidate the structure of the bricks and to remove the excess water, so that all the samples had similar moisture content. Since some of the slag material was found to be agglomerated, this step was also used to homogenize the particle sizes within the samples. The bricks were used for further carbonation tests and ultimately to compare the final product's attributes to the ordinary cement bricks. The machinery used in the forming was Zwick Roell Z010 Universal Testing Machine, shown in Figure 2.

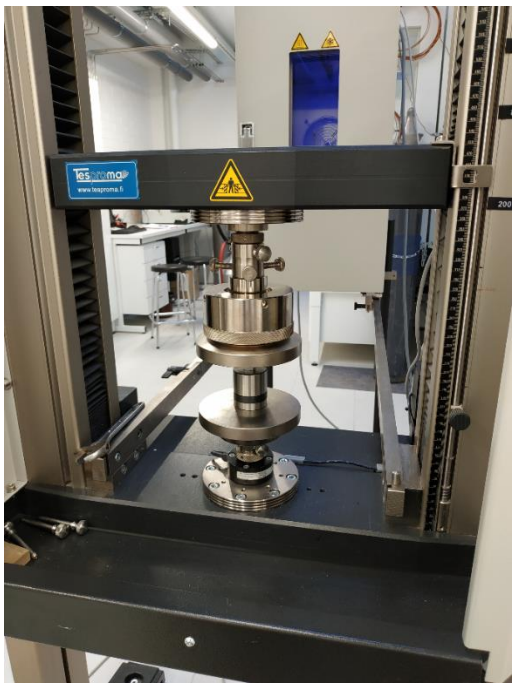

Figure 2. Zwick Roell Z010 Universal Testing Machine, used for sample forming.

1.6 Analysis Methods

To evaluate the characteristics of the finished brick, a number of analysis methods were applied. Since especially the carbon capture was known to have several variables affecting the end product, performing a thorough analysis with different equipment was highly important. The data that was gathered from all the analysis methods was used to further the understanding of the effects, that aluminosilicate based binders and carbonation has to the attributes of a concrete brick.

1.6.1 Unconfined Compressive Strength Test

The most important thing to measure was deemed to be the compression strength of the brick, as it is crucial factor for any construction material. This was tested using Zwick Roell Z010 Universal Testing Machine, with a setting that measures the used force up until the shattering of the sample. The force at the shatter point was then divided with the surface area under stress to determine the compressive strength of the brick. The pressing velocity for this test was 1.8 mm/min and the mold used in the forming of the bricks was 169 mm^2. The results of this test were used to evaluate whether or not the concrete using De-S as a binder could achieve compressive strengths similar to the concrete made with ordinary cement.

1.6.2 Air Jet Sieving

To determine the particle size distribution of the slags used in the samples, Hosokawa Alpine 200LS air jet sieve was used. This measurement method was chosen, since the powdery slag particles had agglomerated to some degree into larger particles, making it difficult to accurately measure the particle sizes. The air jet sieving has an advantage on this kind of materials, as the vacuum combined with a rotating slotted nozzle disperse the particles before drawn to the sieve by the suction. The particle size distribution of the slags can be found in section 2.1 Material Preparing. The picture of the air jet sieve is presented on Figure 3.

Figure 3. Hosokawa Alpine 200LS air jet sieve.

1.6.3 Thermal Gravimetric Analysis

To determine the bricks' thermal stability, a thermal gravimetric analysis (TGA) was used. Thermal stability is important for any construction material, as it describes the degree of decomposition of the micro-structure in the sample when exposed to high temperatures. In TGA, the mass of a sample is measured over time whilst increasing the temperature. This kind of testing provides information about physical phenomena such as phase transitions, absorption, adsorption and desorption. Additionally some chemical phenomena can also be measured, such as chemisorption, thermal decomposition and solid-gas reactions (Coats and Redfern, 1963).

1.6.4 X-Ray Powder Diffraction

The x-ray powder diffraction (XRD), was used to identify the minerals contained in the sample by colliding x-rays to a crystalline material. The x-rays diffract from the sample in a various ways depending on the elements found in the sample material. The diffraction angles of the x-rays are then converted with Fourier transforms into unique d-spacings that can be compared to standardized reference patterns to derive the mineral composition of the sample (Bish and Post, 1989). In more detail, the atoms in the sample are arranged with a distance d. The x-rays then interfere constructively on the path, where 2d sin (θ) is equal to an integer multiple of the wavelength, creating a diffraction maximum in accordance with Bragg's Law (Eq. 5). In the positions where

the waves are out of phase, the waves interfere destructively, creating spaces to the diffraction pattern called atomic spacing (Cullity, 1978).

$$2d \sin \theta = n\lambda, \ n = 1,2, \ldots \quad (5)$$

In Eq. 5 the d is the separation of the waves, θ is the separation angle, n is a positive integer and λ is the wavelength.

1.6.5 X-Ray Fluorescence Spectrometer

To determine the chemical compositions of the slags used in the samples, an x-ray fluorescence spectrometer (XRF) was used. In XRF the sample is exposed to short-wavelength x-rays to ionize its component atoms. The ionization causes one or more electrons of the atom to exit, which makes the atom momentarily unstable. To re-stabilize the atom, the remaining electrons fill the vacant lower orbital, and while doing so, release amount of energy characteristic to the orbital transition. This energy release in the form of photons cause fluorescent radiation, to which a specific wavelength can be calculated using a certain derivation of the Planck's law, shown in Eq. 6.

$$\lambda = \frac{hc}{E} \quad (6)$$

The wavelengths are then separated and sorted to form a spectrum, from which the amount of each element in the sample can be determined according to the intensity of each wavelength (Beckhoff et al., 2006). The units in Eq. 3 are following: the Planck constant (h), a physical constant depicting the quantum of electromagnetic action, relating the energy carried by a photon to its frequency. The speed of light is marked with c and the wavelength is marked with lambda (λ). The E in the equation stands for the energy of the photons relative to the frequency of the radiation (Planck, 1989).

1.6.6 Scanning Electron Microscope

To examine crystal morphologies, a scanning electron microscope (SEM) was used. SEM is a type of electron microscope that is used to produce images of the sample by scanning the surface with a beam of electrons. The electrons interact with the atoms in the sample, producing signals that provide information about the surface topography

and composition. To produce an image of the sample, the electron beam must first be scanned with a raster scan pattern, and the position of the beam has to be combined with the intensity of the received signal. To produce a readable picture from SEM, the samples must be small enough to fit the specimen stage. Additionally, a sample has to withstand the vacuum created during the measurement and it may need special coating to increase its electrical conductivity. A non-conductive sample will collect charge from the electron beam instead of reflecting the electrons, causing the image to be faulty. The resolution from a SEM can optimally be over 1 nm (Stokes, 2008).

2 MATERIALS AND METHODS

The lab work of the present study was divided into an initial phase and an optimization phase. During the initial phase, different compositions and reaction conditions were tested to determine which would yield the specimens with highest compressive strength. When these factors had been solved, smaller variations for the reactions and materials were made to optimize the sample attributes even further. The first step in the sample production was material preparing, consisting of configuring the equipment and mixing the raw materials with different ratios. After that, the mixture was pressed into bricks and cured using a carbonation reaction. The final step was testing the bricks after 14 days of setting time for their compressive strength, thermal stability, crystal structure and chemical composition.

2.1 Material Preparing

The BOF and desulfurization slag samples used in the work were acquired from a local steel factory. In the initial tests desulfurization slag was used as a binder and mixed with aggregate sand (CEN-Normsand EN 196-1). Deionized water was added to turn the mixture into moldable sludge. In each batch the water portion was set to be just enough that some moisture could be seen to seep out from the mold during the pressing step. This was found to be 30-35% of the slag weight depending on the batch. The sand was added to the mixture in varying portions compared to the slag weight, from 0% of sand-to-slag percentage up to 200%.

In the optimization phase the composition of the samples with highest compressive strengths were chosen as a basis for new sample batches. This composition was then carbonated in different conditions. As an additional test, BOF slag was used in some batches instead of the desulfurization slag, using the composition chosen for the optimization phase. This provided data for comparison between BOF and De-S.

To determine the particle size distribution of the slags used for the research, an air jet sieve (Hosokawa Alpine 200LS), with sieve sizes available from 20 µm to 2000 µm

was used. The results for both measurements can be found in Appendix 3. The particle size distributions are also shown as a graph in Figure 4. The grain size distribution for the standardized sand can be found in Appendix 4.

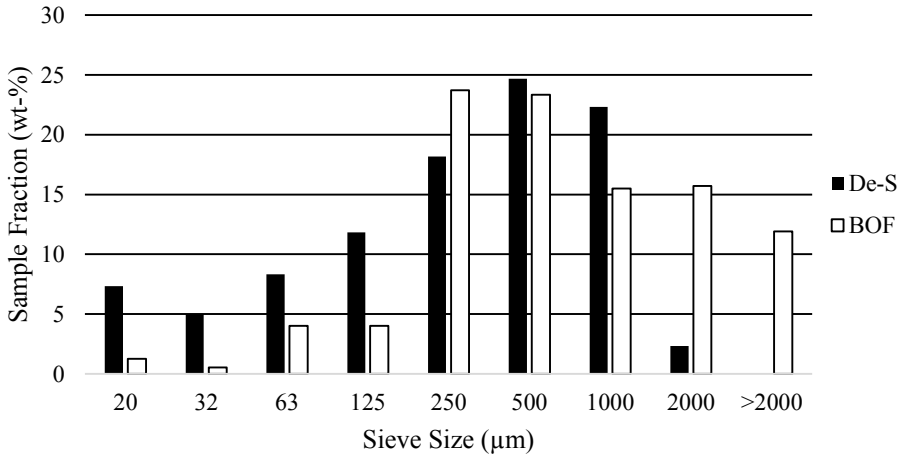

Figure 4. Particle size distribution of slag samples.

2.2 Sample Forming

After the mixture of slag, sand and water had the desired composition, it was set on a mold and pressed 1.8 mm/min, until 20 MPa pressure was reached. This resulted the mixture to form small cubes, convenient for carbonation and later compressive strength testing. The 20 MPa pressure was converted to 3380 N of force for the machine, since the pressing mold was 13 mm × 13 mm = 169 mm^2 in surface area. The conversion is shown on Eq. 7.

$$20\ \text{MPa} = \frac{\text{F}}{\text{A}} \rightarrow \text{F} = 0{,}000169\ \text{m}^2 \cdot 20\ \text{MPa} = 3380\ \text{N} \qquad (7)$$

During the sample forming, the sufficient moisture saturation of the mixture was ensured by adding deionized water to the mixture every time when no moisture could not be seen to seep out of the mold during pressing. The excess water was then dried from the surface before extracting the sample brick from the mold. The pressing mold

equipment is presented in the Figure 5. The bricks removed from the mold are presented in the Figure 6.

Figure 5. Pressing mold equipment.

Figure 6. Batch of bricks before carbon capture.

2.3 Carbon Capture

The carbon capture was done using a steel reactor, which was heated to 150 ^{o}C and pressurized to 6 bar with CO_2. The samples were cured in the reactor for 60 and 120 minutes for each composition in the initial phase, to determine the sufficient curing time. The heating time for the reactor to reach 150 ^{o}C was not included in reaction time. After the samples of the initial phase were carbonated, the strength testing could begin.

After the most suitable sand-to-slag ratio was found via strength tests, the curing time was varied to monitor its effect to compressive strength. The tests were conducted from 15 minute curing to 120 minute curing. To gain comparison data, a batch of samples using BOF as binder instead of De-S was cured for 60 minutes with the same sand-to-slag ratio.

The reactor used for carbonation curing can be found in Picture 6. The reactor had two separate gas inlets for carbon dioxide and nitrogen, as well as pressure monitoring and a heating element. The gas outlet was connected to separate degassing system to ensure operational safety. To ascertain there are no leaks from the reactor, the sealant ring was coated with a Teflon tape. In the Figure 7, the reactor is shown both closed in the left, and opened in the right, to better clarify the operating configuration.

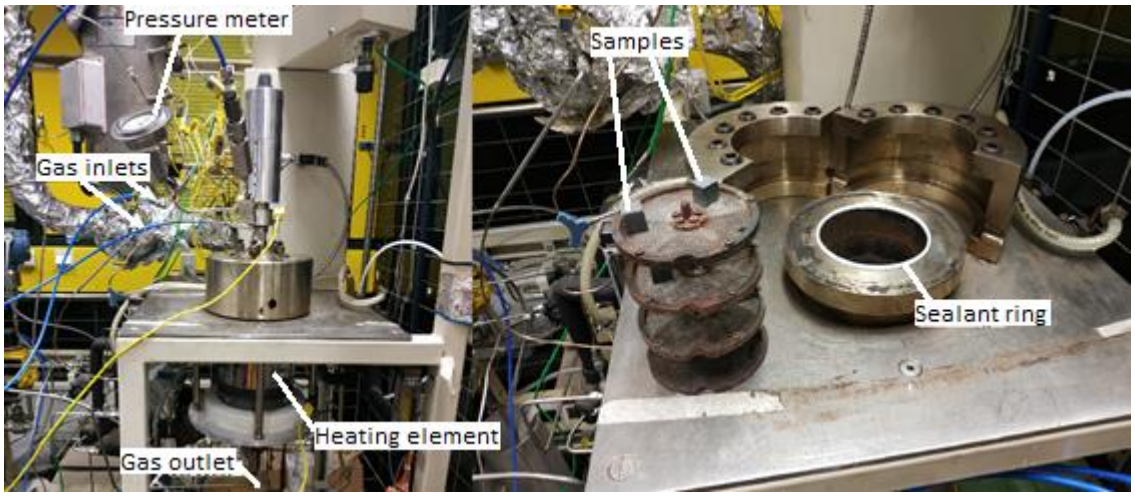

Figure 7. Reactor used for carbonation.

2.3.1 Effects of Carbonation

To provide further information about the effect of carbon capture, batches varying from 0% to 200% sand-to-slag percentage were prepared in otherwise identical conditions, but changing the pressurizing gas from carbon dioxide to nitrogen. This test was also done to a batch of BOF slag to compare the abilities of the different slag types. Nitrogen was decided to fit this purpose well, since it is an inert gas in the reaction conditions used in the present study, and thus does not react to the chemical compounds found in the samples. (McNaught and Wilkinson, 1997).

2.4 Unconfined Compressive Strength Analysis

In order to observe the attributes of the bricks, some of randomly selected specimens of each batch were put into a strength test. This test was performed with the same machine that had been used to press the bricks, but with different settings. The machine was used to increasingly put more pressure on a brick, until the specimen fractured. This shatter point was then recorded and compared to the size of the specimen to determine its compressive strength. The batches which had the highest average capabilities to withstand the pressure were chosen to additional testing in the optimization phase.

The samples were stored in opened zip lock bags for 14 days before the compressive strength tests to let the samples to dry after the autoclaving and to allow a brief setting time for the concrete. The effects hoped to gain from this setting time were a small degree of carbon mineralization from the carbon dioxide found in the room air. This would make the samples more similar to the concrete set in uncontrolled environment and thus more comparable to ordinary concrete. The storage of the samples after the compressive strength tests and before the other analysis methods was roughly two weeks, during which the storing conditions were similar to the setting period.

The strength testing was conducted using Zwick Roell Z010 Universal Testing Machine, with which the sample was pressed 1.8 mm/min, until the sample fractured. Since the test samples were all 13 mm thick, the surface area under stress was used to calculate the breaking pressure. The results from the initial test involving samples with

varying percentage of aggregate and two different curing times can be found from Appendix 5.

2.5 Scanning Electron Microscopy (SEM) Analysis

For the SEM analysis, batches with 0%, 25% and 200% sand-to-slag percentages were deemed the most suitable for crystal structure observations. The samples were ground into powder using a mortar and sputtered with 5 nm platinum coating to prevent charging the samples with the electron beam used in the SEM. After the preparing, the samples were inserted into the Zeiss ULTRA plus FESEM (Field Emission Scanning Electron Microscope), and photographed with 5000X, 20000X, 30000X and 45000X magnifications. The electron microscope is shown in Figure 8.

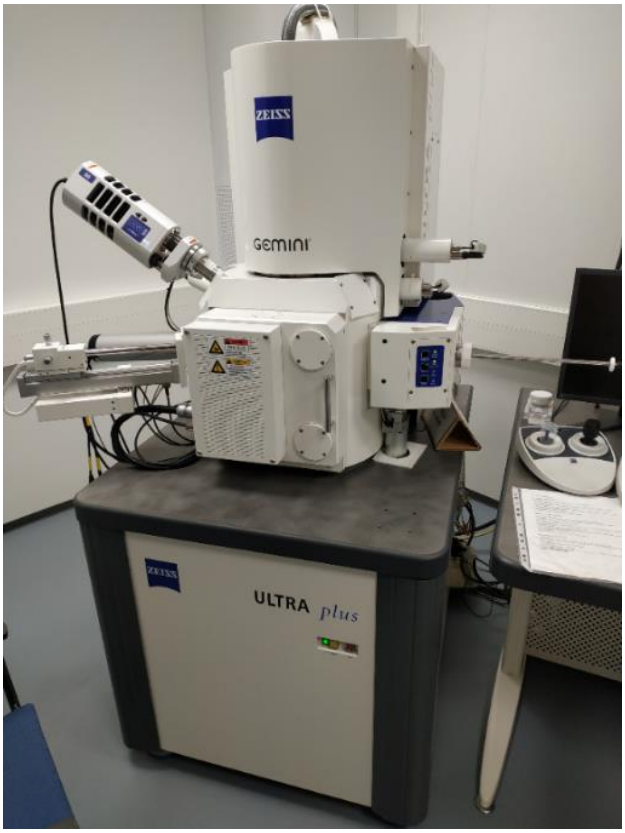

Figure 8. Zeiss ULTRA plus FESEM.

2.6 X-Ray Powder Diffraction (XRD) Analysis

For the XRD analysis, the same samples used earlier in SEM were milled into fine powder using a vibrating disc mill at 700 rpm for one minute in order to have a measurable consistency. After the milling, rutile (TiO_2) was mixed to each sample so that it amounted 10% of each sample weight. This was used as an internal standard when later mapping the mineral peaks of the result data. The model used in this analysis was Rigaku SmartLab 9kW, shown in Figure 9.

Figure 9. Rigaku SmartLab 9kW (XRD).

2.7 Thermogravimetric Analysis (TGA)

For the TGA the previously milled samples were weighed and inserted into ceramic cups, sans the rutile. After this, the samples were heated to 1000 ^{o}C while monitoring the changes in individual sample weights. This provided information about the thermal stability of the samples, as well as some indication about the carbonates within the sample structure. The analysis machine for this step was Precisa prepASH 129, shown in Figure 10.

Figure 10. Precisa prepASH 129 (TGA).

To further analyze the decomposition occurring during the heating of the samples, a derivative thermogravimetry (DTG) curve was calculated from the result data as its first derivative. From the DTG curve the decomposing compounds could be recognized using the XRD data as a reference for possible minerals in set temperature range (Collier, 2016).

3 RESULTS

The laboratory work was split into two main phases, both explained more in detail in chapter 2 Materials and Methods. The first phase included more general testing, as the goal was to determine an approximate sample composition and reaction conditions before more detailed testing. In the second phase, the compressive strength testing was combined with mineralogy analysis, thermal stability testing and electron microscope imaging. The compressive strength testing of the first phase was conducted in the Fibre and Particle Engineering Unit's laboratories, as well as the TGA analysis in the second phase. The XRD and SEM were carried out in the Center of Microscopy and Nanotechnology.

3.1 Unconfined Compressive Strength

The goal for this test phase was to find the most resilient composition of slag powder and sand, along with the most favorable curing time. Once these factors were determined, additional samples were made and further attribute testing scheduled. As described in chapter 2.4 Unconfined Compressive Strength Analysis, with all the samples tested for their compressive strength, a setting time of 14 days was applied. During the setting the samples were stored in opened zip lock bags in room temperature to allow the concrete to harden and dry.

The batch including only De-S and water had an average compressive strength of roughly 14 MPa, with slightly higher strengths recorded with the batch of 120 minute curing time. With 25% aggregate to binder percentage, the compressive strength was the greatest among the batches, especially with 60 minute curing time. The average compressive strength of 22 MPa with the 25%/60 min sample was much higher than could be anticipated, especially considering that when inspecting the trend in Figure 11, roughly 14-15 MPa could be expected. Such compressive strength could not be achieved on the second phase when a sample with identical conditions was made, and thus the reason for this unexpectedly stronger sample batch could not be concluded.

The batch with 100% aggregate to binder percentage had similar compressive strength compared to the 0% and 50% batches, with each having an average compressive strength of 13-15 MPa. The 200% batch was clearly the weakest with its average compressive strength of roughly 7.5 MPa. The compressive strengths for all the De-S batches are presented in Figure 11.

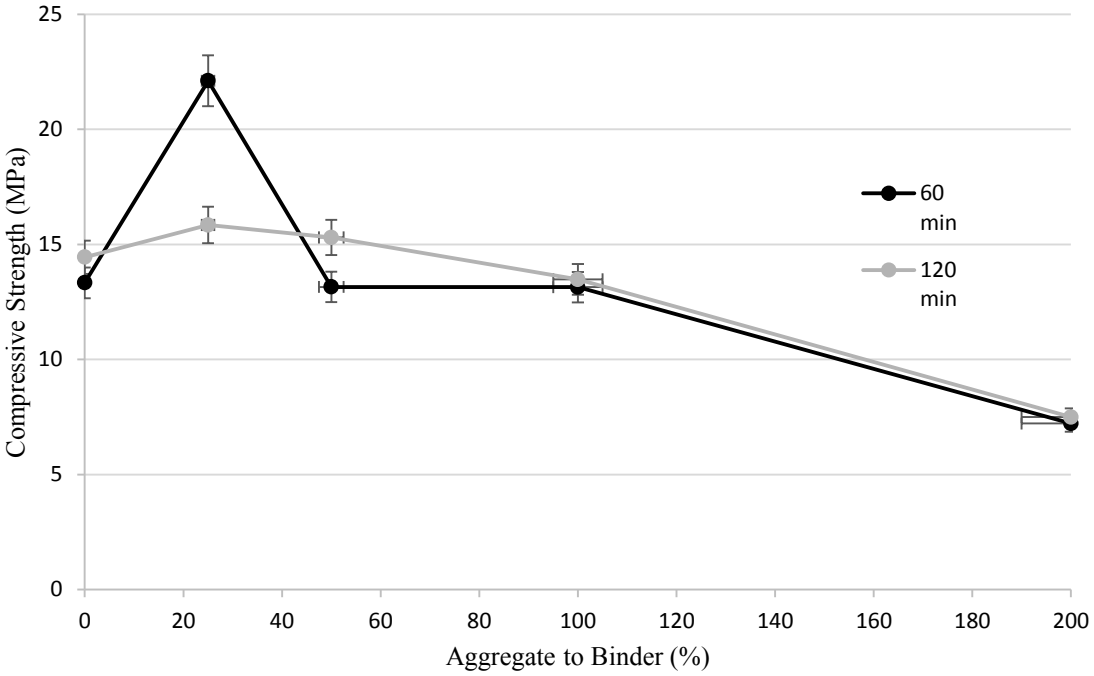

Figure 11. Compressive strengths for initial sample batches.

In the Figure 11, the compressive strengths can be seen to slightly increase with longer curing time with most aggregate amounts. The compressive strength of the strongest samples are close to the requirements for lightest building concrete types used in Finland, even though the standardized testing samples are over ten times thicker (150 mm) and shaped as structurally more durable cylinder, compared to the 13 mm thick cubic shape (Palolahti et al., 2011).

3.2 Curing Time Optimization

To improve the economy of the curing step, a set of batches was prepared for different curing times. The goal for this experiment was to find whether a batch with applicable compressive strength could be produced with much shorter curing times than in the initial phase. This would naturally increase the theoretical production rate and improve the economic feasibility of De-S brick production. The result data for this testing can be found in Appendix 6.

The compressive strengths remained similar during all the curing times up until 120 minute curing, which made the sample bricks slightly stronger. The trend in Figure 12 supports the results gained in the initial phase with other aggregate to binder percentages than 25%, that 120 curing time produces slightly stronger samples compared to 60 minute carbonation. The different compressive strengths are compared as a graph in Figure 12.

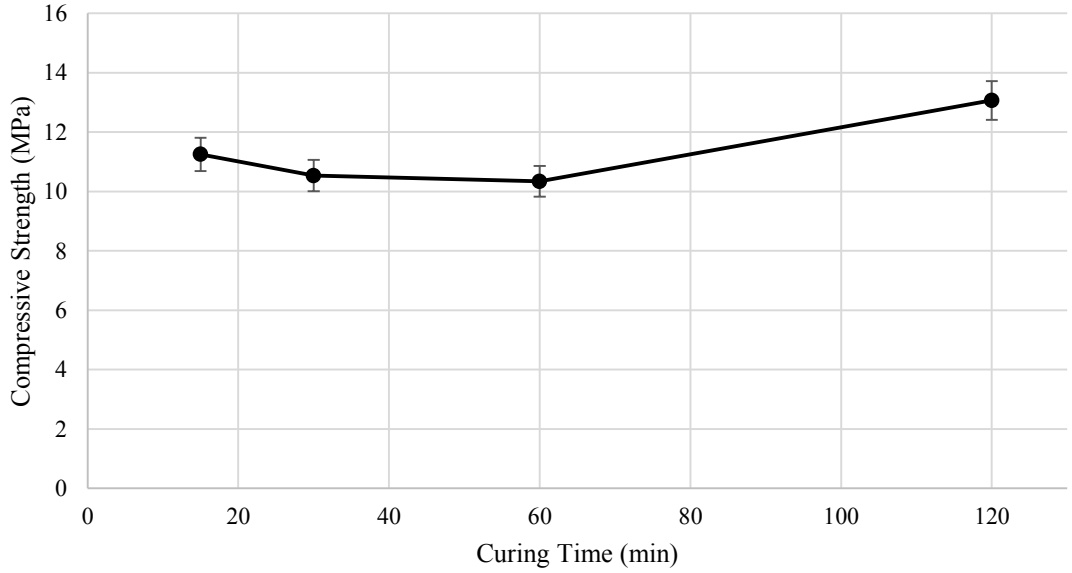

Figure 12. Compressive strengths of the samples with different curing times (De-S).

All of the test batches presented in Figure 12 can be seen to exceed 10 MPa, which can be considered to be a good result, since the test samples were only 13 mm thick. As a comparison, the concrete recommended for building in Finland usually has 25-40 MPa

compressive strength for 150 mm thick cylinder depending on its use (Palolahti et al., 2011).

3.3 Non-Carbonated Samples

After the strength tests had been done for the initial sample batches, a set of control batches was prepared to monitor the effects of carbonation. These samples were cured in a reactor pressurized only with nitrogen for the duration of 60 minutes. The results for these test can be found in Appendix 7.

The compressive strengths of the non-carbonated samples are presented as a graph in Figure 13. The trend in Figure 13 confirms the data gained from the initial phase, that 25% of aggregate to binder was the strongest mixture. The trend also shows the importance of the carbon mineralization for the compressive strength, as the carbonated samples showed 5-10 times higher compressive strengths than the non-carbonated ones.

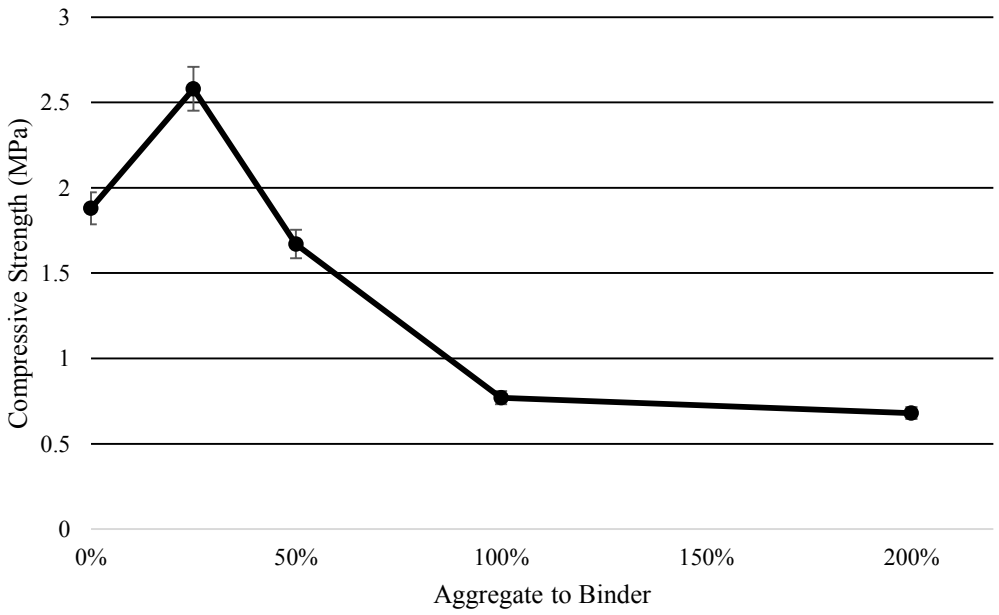

Figure 13. Compressive strengths of non-carbonated De-S samples as a function of aggregate amount.

Figure 13 shows that the highest compressive strength of 2.6 MPa was gained at 25% aggregate to binder percentage, after which the strength dropped sharply to 0.7 MPa. The difference to the carbonated samples was evident with the workability of the bricks

as well, with the non-carbonated samples crumbling during already during the setting time and carbonated ones keeping their structure intact.

3.4 Chemical Composition

The main tools to determine the chemical composition of different samples were XRD and TGA. The XRD provided the intensity of individual reflections, originating from the mineral lattice interaction with the X-ray beam was used to analyze the mineralogical composition of the samples. The data gained from the TGA could be used to monitor different compounds according to the individual decomposition temperatures of different mineral phases found in the samples. The data collected from these measurement was compared to the raw material composition gained from the XRF analysis done in the initial phase.

The composition of the samples was found to be close to what was predicted, with different calcium carbonate phases produced during the carbonation being the main components. On the other hand, the samples were found to have complex mineral composition, with XRD signal having many small peaks along the spectrum. This was supported by various crystal structures found in SEM images. This suggests that the samples formed amorphous structures in some instances, in which no individual crystal type dominates the specimen surface but instead several different formations can be found.

3.4.1 XRD Analysis

The data signal received from the x-ray powder diffraction (XRD) analysis is shown in Figure 14. In the figure all the individual sample signals are separated for easier interpretation. The different mineral peaks found in the data are marked with letters, with most notable peaks marked with dashing to ease comparison between different signals. Some peaks overlap and some peaks are caused as a combination of minerals. These are marked with &-symbol for overlapping and with /-symbol for combined minerals.

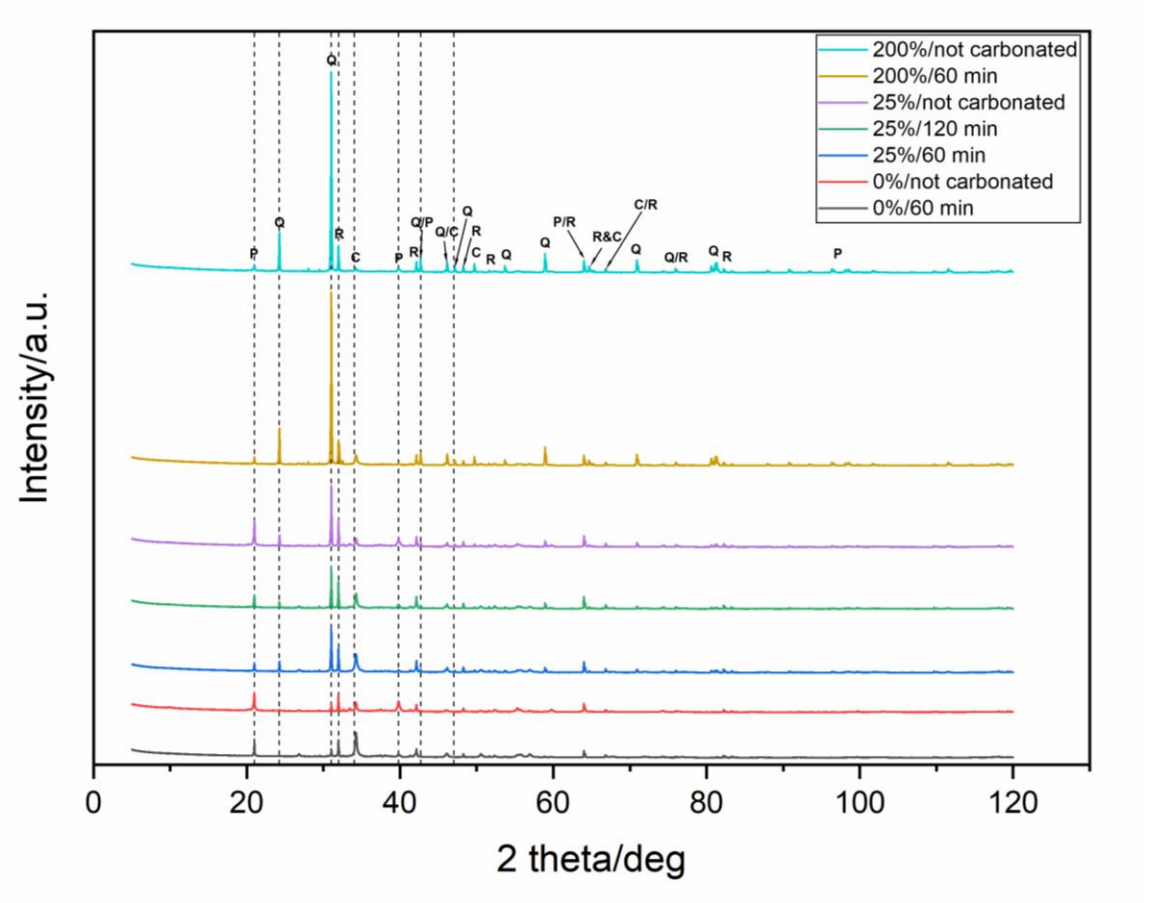

Figure 14. XRD data graph.

Of these minerals, the portlandite (P) is presumed to originate from the slag and the calcite (C) to be a product of the carbonation. This presumption is based on the higher intensity peaks of P in non-carbonated samples than in carbonated ones. The opposite trend can be seen with C peaks. Quartz (Q) peaks can be found to decrease in intensity as the ratio of sand decreases. The rutile (R) peaks can be used to compare the intensities of the other peaks, since it is known to be added 10% of the sample weight before the analysis. It should be noted however, that the intensities and positions of the reflection peaks are not exact, since the smoothness of the sample surface and particle size can affect it.

Since the peaks can be found in the same positions in each sample signal, some conclusions can be drawn from the data concerning the mineral composition. This is true especially, if the data is compared with TGA data and the pictures received from the SEM analysis. The minerals were recognized from the XRD data signal by reviewing the XRF data of the De-S, and comparing the compounds found by XRF to

the potential minerals causing the peaks. This method yielded mineral identifications that are consistent with TGA and SEM findings.

3.4.2 Thermogravimetric Analysis

In the thermal gravimetric analysis (TGA) the samples were heated to 1000 ^{o}C while measuring the changes in the sample masses. The data collected is presented on Figure 15.

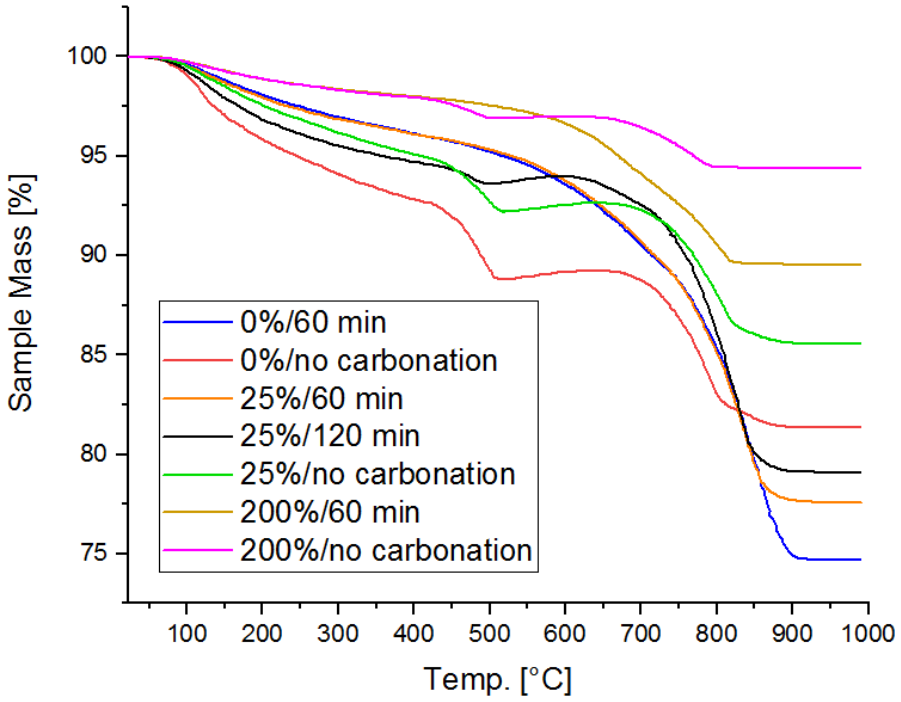

Figure 15. TGA data curve.

In Figure 15 the thermal stabilities of the samples can be seen to follow the ratio of sand. This can be expected due to the high amounts of thermally stable quartz found in the sand containing samples during the XRD analysis. The more carbonated samples can be seen to lose more mass during the heating, which can be explained by decomposing calcium carbonate formations. The thermal decomposition (or calcination) products of calcium carbonate are typically calcium oxide and carbon dioxide (Al Omari et al., 2016). The decomposition reaction is presented in Eq. 8.

$$CaCO_3(s) \rightarrow CaO(s) + CO_2(g) + 178\ kJ/mol \quad (8)$$

Further analysis of the decomposing compounds can be made using the derivative thermogravimetry (DTG), in which the first derivative of the TGA data can be used to determine the decomposing phases. From the DTG curve, local minimum values can be differentiated, which each represent an identifiable mineral phase decomposition. According to the results found from the XRD analysis, at least calcite and portlandite could be expected to be found from the DTG curve. The DTG graph is presented in Figure 16.

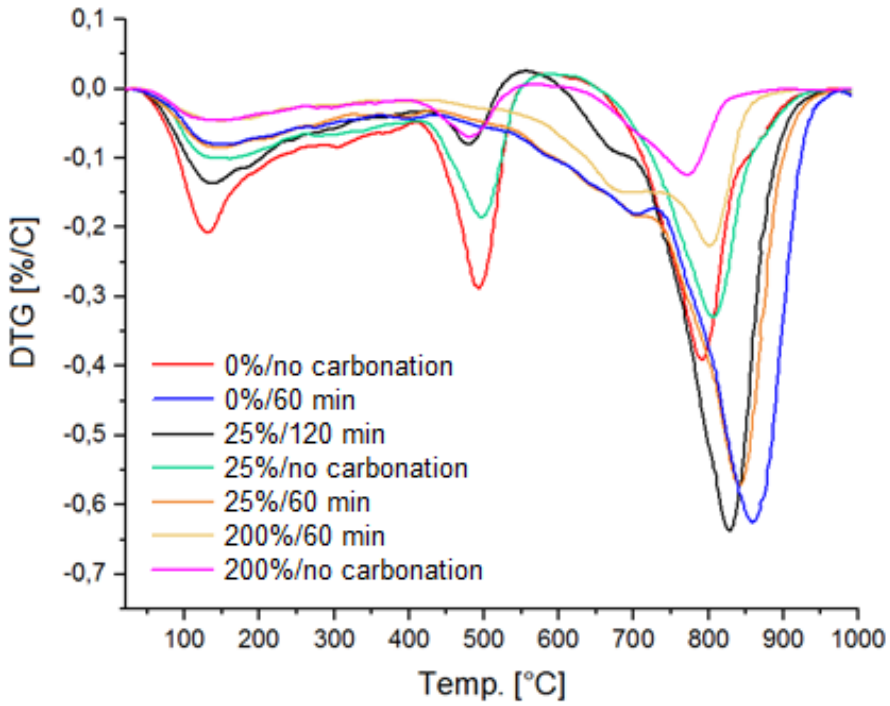

Figure 16. DTG data curve.

In Figure 16, three main areas can be seen in which major amounts of mass loss occurs. These areas are 100-200 ^{o}C, 450-550 ^{o}C and 750-900 ^{o}C. The mass loss areas found in the data are wide, which is interpreted to mean that there are several overlapping minerals decomposing simultaneously. This increases the amount of possible interpretations of the phases, though the main components can be identified with adequate accuracy using the XRF and XRD data as a basis for the compounds sought from the data. Additionally, certain amorphous phases could be expected to be found, such as portlandite ($Ca(OH)_2$), C-S-H, as well as crystalline calcite ($CaCO_3$).

The first decomposed phase contains water at 100 ^{o}C, along with calcium carbonate likely in a form of ettringite ($Ca_6Al_2(SO_4)_3(OH)_{12}\cdot 26H_2O$), considering its decomposition temperature of 140 ^{o}C and natural occurrence in concrete materials. The middle phase at 450-550 ^{o}C contains mostly calcium silicate hydrate (C-S-H), considering its decomposition temperature of 500 ^{o}C and expected presence in the samples. The decomposition of portlandite occurs likewise in temperatures of 400-500 ^{o}C, which makes it likely an overlapping phase decomposing in the area. The last area fits typical decomposition temperatures of calcite isomorphs aragonite and vaterite, though the area is wider than the others and can hence contain different minerals for separate samples (Collier, 2016; Gartner et. al, 2011).

3.5 SEM Analysis

To further analyze the mineral phases identified in the XRD and TGA data, scanning electron microscope imaging was used. SEM analysis corroborated the findings, revealing several kind of crystals consistent with the shape of different calcium carbonate minerals. In the sample containing just De-S and water and with 60 minute carbonation the crystals show mostly shapes associated with C-S-H and calcite (Figure 17). The fuzzier shapes (a) seen in Figure 17 are assumed to be C-S-H and the more cubic crystals (b) calcite. According to the XRD data and literary comparison (Mydin, 2017) the cubic crystals may also be portlandite, which shares similar crystal structure with calcite.

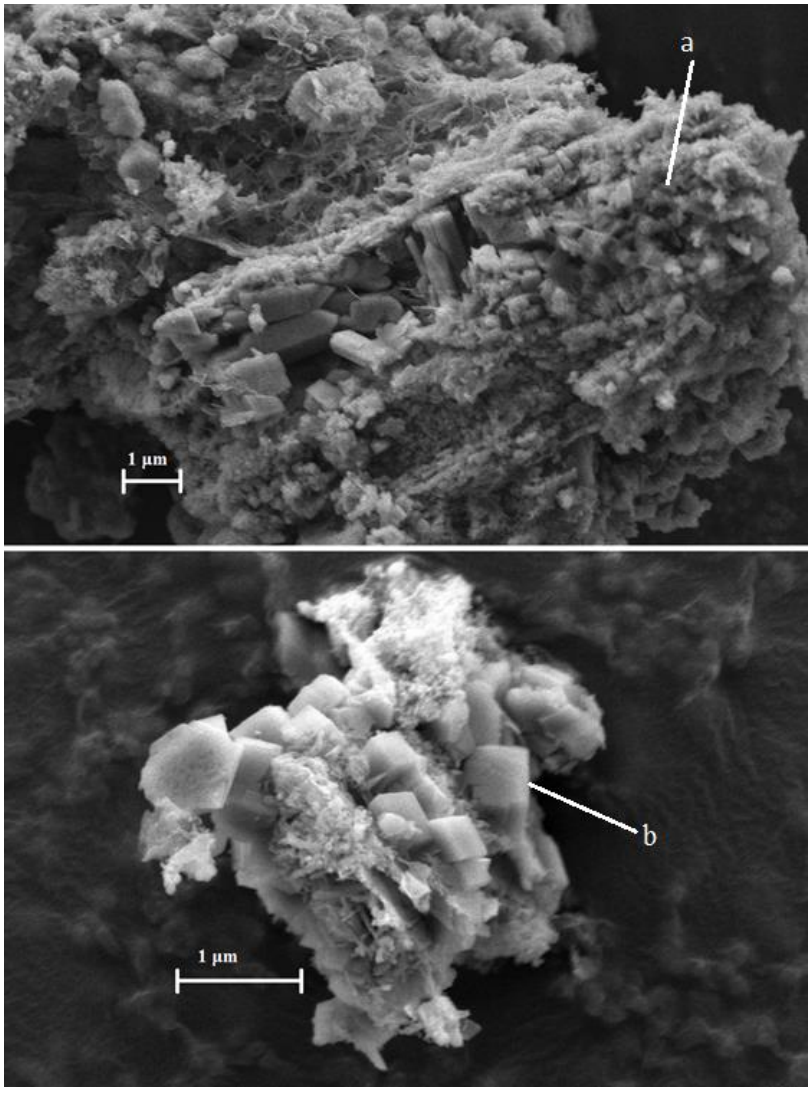

Figure 17. SEM image of De-S, 0% sand with 60 min carbonation.

In De-S, 0% sand with no carbonation (Figure 18) the sharp shapes seen are likely ettringite, found also in other samples but with particular representation in the sample with no aggregate or carbonation used. The difference to the identical sample with 60 minute carbonation is striking, as only small measure of ettringite was found on the carbonated sample. In XRD analysis the non-carbonated sample with 0% aggregate showed much lower intensity with calcite peak, which indicates the major role of carbonation with the formation of calcite crystals. The non-carbonated sample also decomposed in notably lower temperature during the TGA analysis compared to the carbonated sample, which suggests improved thermal stability as an effect of the carbonation. When comparing the DTG and the XRD data with the non-carbonated sample, portlandite should be present along with the ettringite findings.

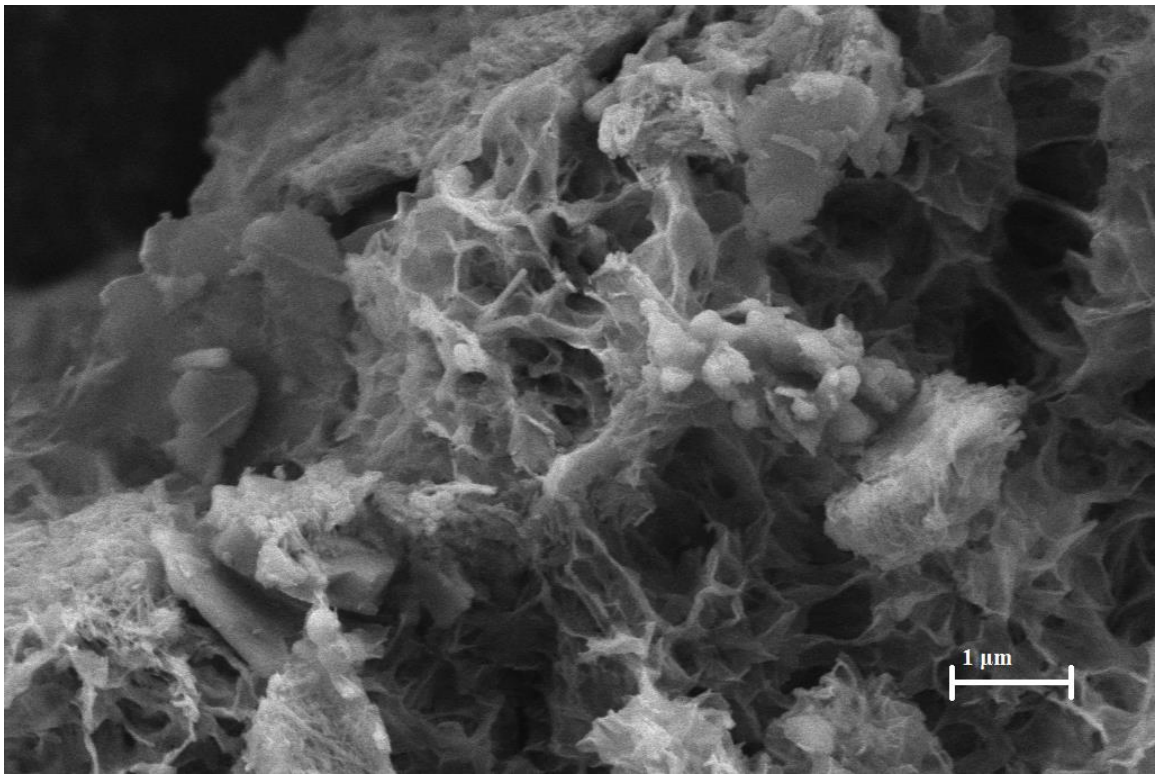

Figure 18. SEM image of De-S, 0% sand with no carbonation.

In De-S, 25% sand with 120 min carbonation (Figure 19), the flaky crystals are portlandite, covered with fuzzy C-S-H crystals. The similarity of Figure 19 to the SEM images found in the research of Rochelle et al. is apparent (2004). According to the DTG findings, it is expected that aragonite and vaterite are present due to the decomposition of the 25%/120 min sample mostly decomposing at the higher end of the temperature range in TGA. These phases are more varying in their crystal formations than the more easily recognizable portlandite and C-S-H however, so the SEM images are difficult to use to confirm these occurrences. The XRD data does not show any notable peaks that would differentiate the sample from the one with 60 minute carbonation. The TGA data also follows the curve of the sample with 60 minute carbonation time, which suggests that the additional 60 minutes of carbonation has only limited effect on the thermal stability of the sample.

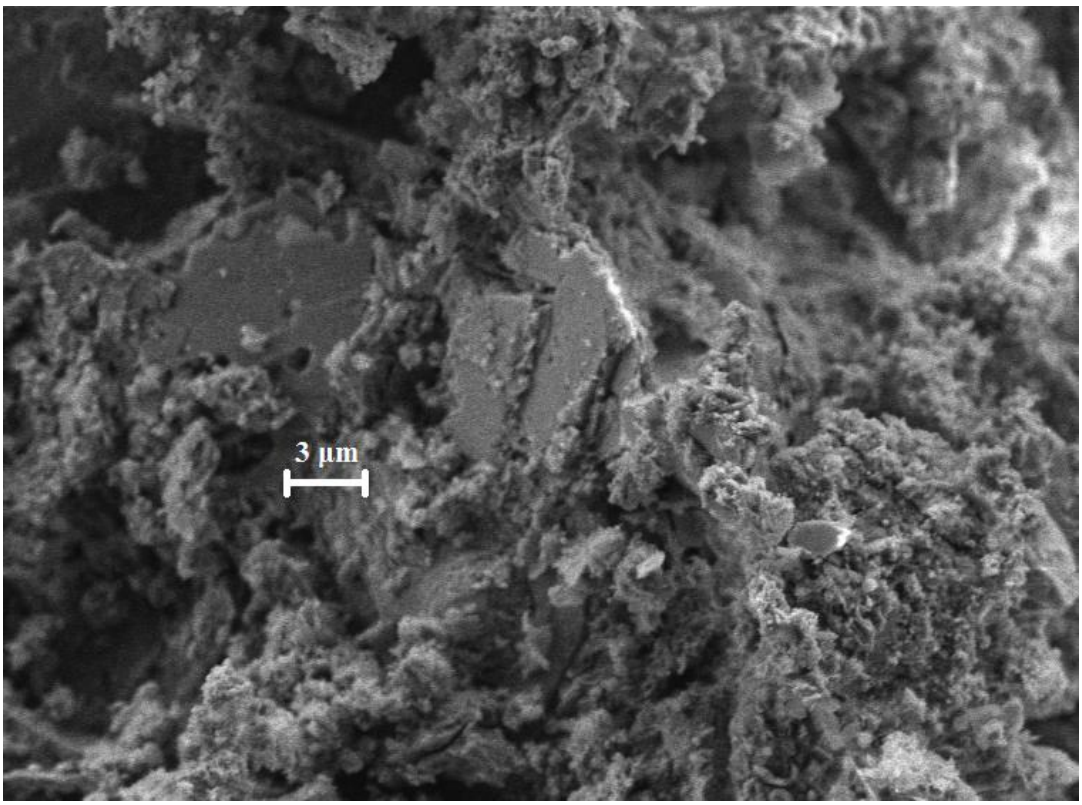

Figure 19. SEM image of De-S, 25% sand with 120 min carbonation.

The crystals found in De-S. 25% sand with no carbonation (Figure 20) are numerous, which would suggest amorphous structure with no dominance of singular crystal shape. The XRD data shows heightened intensity in the peaks showing quartz and portlandite, which is expected considering the lack of carbonation with this sample and the addition of sand. The thermal stability of the 25% sample with no carbonation is average among the samples. This finding was logical considering the SEM imaging with several different formations that would decompose evenly during the TGA.

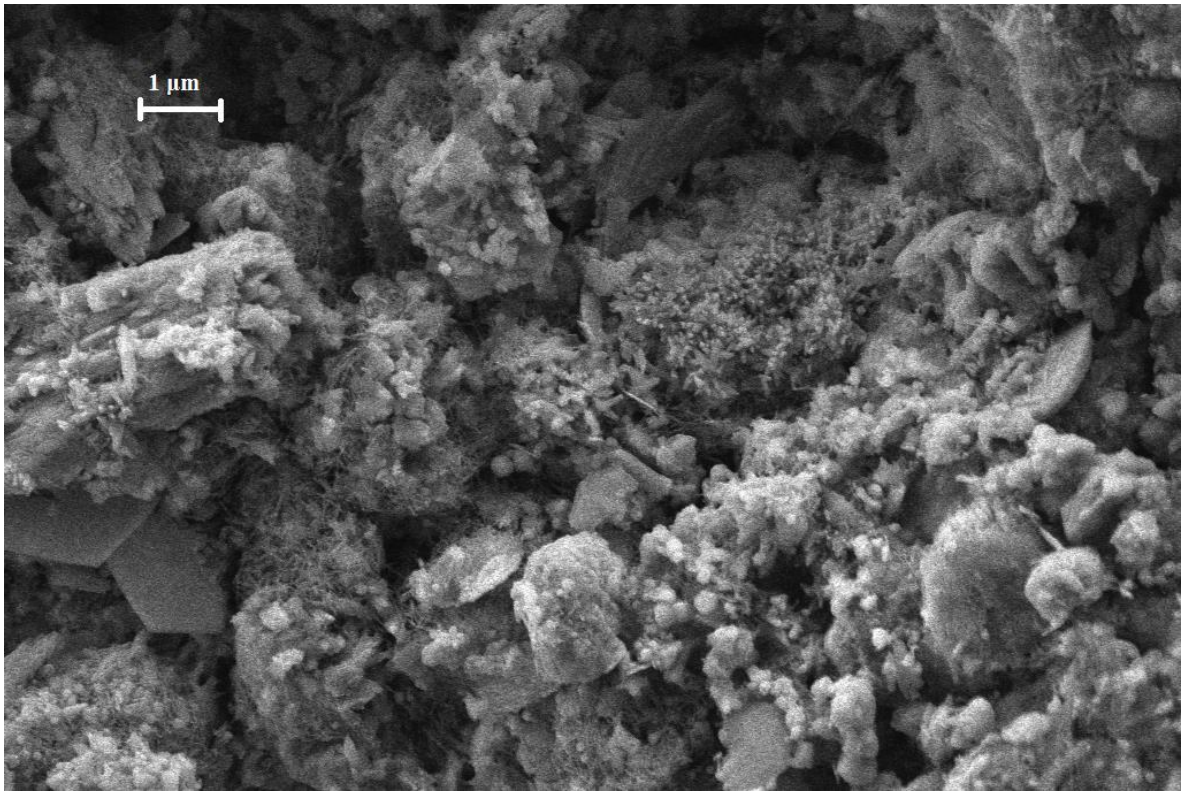

Figure 20. SEM image of De-S, 25% sand with no carbonation.

In De-S, 200% sand with no carbonation (Figure 21) some of the crystals are needle like, and some quartz crystals can be seen as well. Many of the calcium carbonate minerals have been found to produce needle shaped crystals, which makes accurate identification challenging in this case. The thermal stability was highest with the sample with 200% aggregate and no carbonation, which showcases the thermal stability of the quartz found in the aggregate sand.

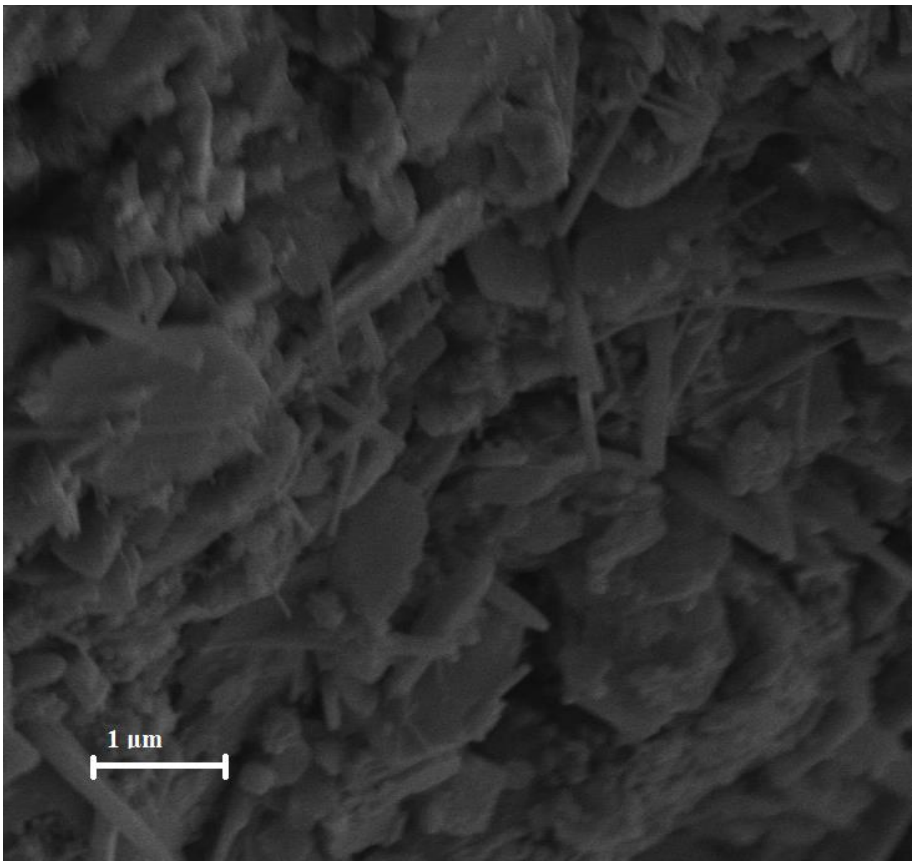

Figure 21. SEM image of De-S, 200% sand with no carbonation.

The XRD data shows only minor peaks apart from the quartz, and any decomposition seen in DTG is almost marginal. When this sample type was carbonated, the thermal stability improved up until 600 ^{o}C, when the calcite formations started to decompose. This suggests that even with high amounts of sand added, the carbon mineralization improves the thermal stability in the lower end of the temperature spectrum in the TGA.

3.6 BOF Samples

To compare the effect of different slag types for the attributes of the sample bricks, BOF slag was used as a replacement of desulphurization slag in otherwise identical conditions. In the first set of experiments, a non-carbonated BOF was tested with and without the CO_2 curing. Since the resulting bricks had drastically lower compressive strength compared to De-S samples, a similar batch with carbonated BOF was prepared. The sand-to-slag percentage of these samples was 25% for each, since it had yielded the most resilient samples with De-S. The strengths of these samples, however, proved to be drastically inferior to the De-S samples, causing the main focus to shift into the De-S analysis. The results of the BOF strength tests can be found in Appendix 8.

4 DISCUSSION AND CONCLUSIONS

The results yielded from this study were promising, and providing a potential option for the re-use of De-S. Especially the increase of up to 20 MPa in compressive strength achieved with only 60 minutes of carbon dioxide pressurizing proved the potential of CCU applications. These results suggest that carbonated De-S concrete can reach the compressive strength required in some applications, notably bricks. Naturally the stability of this concrete should still be investigated in different environments and setting times. The main goals were met, by showing that the De-S is indeed viable binder material for concrete and that carbon capturing can improve the durability of a building material even in mild conditions and short reaction time.

When the results of this study are compared to the research of Cicek and Tanriverdi, similar findings could be made with optimal sand addition (2007). The autoclave pressure in the present study was roughly half of the pressure used in their research, and reaction time was 4-5 hours shorter. However, the compressive strengths found in the specimens of the present study were higher, with smaller and structurally weaker samples matching the strongest samples made by Cicek and Tanriverdi. This suggests that De-S shows higher potential as a binder material compared to fly ash.

An interesting variation in results could be found between different amounts of sand, not to mention the difference between De-S and BOF, despite their chemical composition being close to one another. The most striking difference between De-S and BOF is the coarse nature of BOF, which can explain its poor performance. A research exploring an optimal particle size might shed light to this issue. Additional research topics concerning De-S as building raw material and CCU might include using chemical additives to further improve the carbonation kinetics, along with optimizing the process temperature and pressure with more in depth testing than this study allowed. The stability of the bricks should also be tested in different moisture environments, including long term durability in harsh conditions.

As a summary, the following conclusions were drawn based on the results:

1) The De-S bricks provide comparable attributes to the ordinary concrete for low strength applications.
2) The best compressive strength for the De-S bricks was gained with 25% of aggregate.
3) Carbon mineralization improves both the compressive strength and thermal stability of the De-S bricks.
4) Good quality De-S bricks can be produced in relatively low temperature and pressure with relatively short carbonation time.

5 REFERENCES

Al Omari Mahmoud, Rashid Iyad, Qinna Nidal, Jaber A. and Badwan Adnan, 2016. Chapter Two – Calcium Carbonate. Profiles of Drug Substances, Excipients and Related Methodology 41: 31-132.

Baciocchi Renato, Costa Giulia, Lategano Emanuele, Marini Carlo, Polettini Alessandra, Pomi Raffaella, Postorino Paolo and Rocca Stefania, 2010. Accelerated carbonation of different size fractions of bottom ash from RDF incineration. Waste Management 30 (7): 1310-1317.

Bauer Markus, Gassen Niklas, Stanjek Helge and Peiffer Stefan, 2011. Carbonation of lignite fly ash at ambient T and P in a semi-dry reaction system for CO_2 sequestration. Applied Geochemistry 26 (8): 1502-1512.

Beckhoff Burkhard, Kanngiesser Birgit, Langhoff Norbert, Wedell Reiner and Wolff Helmut, 2006. Handbook of Practical X-Ray Fluorescence Analysis. Springer Science and Business Media. ISBN 3-540-28603-9.

Bish David and Post Jeffrey, 1989. Modern Powder Diffraction. Reviews in Mineralogy 20. Mineralogical Society of America.

Bodor Marius, Santos Rafael, Kriskova Lubica, Elsen Jan, Vlad Maria and Van Gerven Tom, 2013. Susceptibility of mineral phases of steel slags towards carbonation: mineralogical, morphological and chemical assessment. European Journal of Mineralogy 25 (4): 533-549.

Carroll John, Slupsky John and Mather Alan, 1991. The Solubility of Carbon Dioxide in Water at Low Pressure. Journal of Physical and Chemical Reference Data 20 (6): 1201-1209.

Chen Ying-Liang, Chang Juu-En and Ko Ming-Sheng, 2017. Reusing Desulfurization Slag in Cement Clinker Production and the Influence on the Formation of Clinker Phases. Sustainability 9 (9): 1585.

Chen Ying-Liang, Ko Ming-Sheng, Chang Juu-En and Lin Chun-Ta, 2018. Recycling of desulfurization slag for the production of autoclaved aerated concrete. Construction and Building Materials 158: 132-140.

Cicek Tayfun and Tanriverdi Mehmet, 2007. Lime based steam autoclaved fly ash bricks. Construction and Building Materials 21 (6): 1295-1300.

Coats A.W. and Redfern J.P., 1963. Thermogravimetric analysis. A review. Analyst 1053 (88): 906-924.

Collier Nick, 2016. Transition and Decomposition Temperatures of Cement Phases – A Collection of Thermal Analysis Data. Ceramics-Silikáty 60 (4): 338-343.

Cuéllar-Franca Rosa and Azapagic Adisa, 2015. Carbon capture, storage and utilisation technologies: A critical analysis and comparison of their life cycle environmental impacts. Journal of CO_2 Utilization 9: 82-102.

Cullity B.D., 1978. Elements of X-ray Diffraction. Addison-Wesley. ISBN 0-201-01174-3.

Criado Maria, Xinyuan Ke, Provis Jogn and Bernal Susan, 2017. Alternative inorganic binders based on alkali-activated metallurgical slags. Sustainable and Nonconventional Construction Materials using Inorganic Bonded Fiber Composites: 185-220. Woodhead Publishing. ISBN 978-0-08-102001-2.

Fruehan Richard, 1998. The Making, Shaping, and Treating of Steel. Steelmaking and Refining Volume, 11th edition: 10. The AISE Steel Foundation. ISBN 0-930767-02-0.

García-Lodeiro Inés, Palomo Angel and Fernández-Jiménez Ana, 2015. An overview of the chemistry of alkali-activated cement-based binders. Handbook of Alkali Activated Cements, Mortars and Concretes: 19-47.

Gartner Ellis, Walenta Günther, Morin Vincent, Termkhajornkit Pipat, Baco Isabelle and Casabonne Jean-Michelle, 2011. Hydration of a Belite-CalciumSulfoaluminate-Ferrite cement: AetherTM. 13th International Congress on the Chemistry of Cement, Madrid, Spain.

Glukhovsky Victor, 1994. Ancient, modern and future concretes. Proceedings of the First International Conference on Alkaline Cements and Concretes. Kiev, Ukraine.

Goldman Lee, 2007. Principles of CT and CT Technology. Journal of Nuclear Medicine Technology 35 (3): 115-128.

Huang Li-Jeng, Wang Her-Yung and Wei Chih-Ting, 2016. Engineering properties of controlled low strength desulfurization slags (CLSDS). Construction and Building Materials 115: 6-12.

Huijgen Wouter, Witkamp Geert-Jan and Comans Rob, 2005. Mineral CO_2 Sequestration by Steel Slag Carbonation. Environmental Science and Technology 39 (24): 9676-9682.

Krivenko Pavel, 1994. Alkaline cements. Proceedings of the First International Conference on Alkaline Cements and Concretes. Kiev, Ukraine.

Kurtis Kimberly, 2017. Portland Cement Hydration. School of Civil Engineering, Georgia Institute of Technology. Atlanta, Georgia, United States of America.

Lackner Klaus, 2003. A Guide to CO_2 Sequestration. Science 300 (5626): 1677-1678.

Larachi Faical, Gravel J.-P., Grandjean Bernard and Beaudoin Georges, 2012. Role of steam, hydrogen and pretreatment in chrysotile gas–solid carbonation: Opportunities for pre-combustion CO_2 capture. International Journal of Greenhouse Gas Control 6: 69-76.

Locher Friedrich, 2006. Cement: Principles of production and use. Verlag Bau und Technik, Düsseldorf, Germany. ISBN 3-7640-0420-7.

McNaught A.D. and Wilkinson A., 1997. IUPAC. Compendium of Chemical Terminology, 2nd edition. Blackwell Scientific Publications, Oxford. ISBN 0-86542-684-8.

Miller Sabbie, Vanderley John, Pacca Sergio and Horvath Arpad, 2018. Carbon dioxide reduction potential in the global cement industry by 2050. Cement and Concrete Research 114: 115-124.

Montgomery D. and Wang G, 1993. Engineering uses of steel slag-A by-product material. Proceedings of the International Conference on Environmental Management-Geo-Water and Engineering Aspects.

Mydin Azree, 2017. Preliminary Studies on the Development of Lime-based Mortar with Added Egg White. International Journal of Technology 8 (5): 800.

Nisbet Michael, Marceau Medgar and Van Geem Martha, 2002. Environmental Life Cycle Inventory of Portland Cement Concrete. Portland Cement Association: Research and Development Information. Serial Number 2137a.

Pal Suman, Mukherjee Abhijit and Pathak Snehal, 2003. Investigation of hydraulic activity of ground granulated blast furnace slag in concrete. Cement and Concrete Research 33 (9): 1481-1486.

Palolahti Tuomas, Petrow Seppo and Mannonen Petri. 2011. Pienrakentajan betoniopas. Betoniteollisuus ry. ISBN 978-952-269-018-0.

Peng-Guan Li and Zhao Feng-Qing, 2016. Autoclaved Brick from Volume-Stability-Modified Steel Slag and Low Silicon Tailings. MATEC Web of Conferences 67 (05015). International Symposium on Materials Application and Engineering (SMAE 2016).

Planck Max, 1989. The Theory of Heat Radiation. History of Modern Physics and Astronomy 11 (1). AIP-Press. ISBN 978-0-88318-597-1.

Polettini Alessandra, Pomi Raffaella and Stramazzo Alessio, 2016. CO_2 sequestration through aqueous accelerated carbonation of BOF slag: A factorial study of parameters effects. Journal of Environmental Management 167: 185-195.

Proctor Deborah, Fehling Kurt, Shay Erin, Wittenborn J., Green J., Avent C., Bigham R., Connolly M., Lee B., Shepker Thomas and Zak Margaret, 2000. Physical and chemical characteristics of blast furnace, basic oxygen furnace, and electric arc furnace steel industry slags. Environmental Science and Technology 34 (8): 1576-1582.

Provis John and Van Deventer Jannie, 2009. Geopolymers: structures, processing, properties and industrial applications. Woodhead Publishing Limited. ISBN 978-1-845-69449-4.

Rochelle Christopher, Milodowski Antoni and Czernichowski-Lauriol Isabelle, 2004. The impact of chemical reactions on CO_2 storage in geological formations: A brief review. Geological Society London Special Publications 233 (1): 87-106.

Santos Rafael and Van Gerven Tom, 2011. Process intensification routes for mineral carbonation. Greenhouse Gases: Science and Technology 1 (4): 287-293.

Santos Rafael, Ling Da, Sarvaramini Amin, Guo Muxing, Elsen Jan, Larachi Faical, Beaudoin Georges, Blanpain Bart and Van Gerven Tom, 2012. Stabilization of basic oxygen furnace slag by hot-stage carbonation treatment. Chemical Engineering Journal 203: 239-250.

Schuiling Roelof, 2011. Olivine against climate change and ocean acidification. Semantic Scholar. URL: [http://www.innovationconcepts.eu/res/literatuurSchuiling/olivineagainst climatechange23.pdf]. Cited 15.7.2019.

Sedjo Roger and Sohngen Brent, 2012. Carbon Sequestration in Forests and Soils. Annual Review of Resource Economics 4: 127-144.

Shi Caijun, Krivenko Pavel and Roy Della, 2003. Alkali-Activated Cements and Concretes. Taylor and Francis, London.

Shu-Yuan Pan, Kinjal Shah, Yi-Hung Chen, Ming-Huang Wang and Pen-Chi Chiang, 2017. Deployment of Accelerated Carbonation Using Alkaline Solid Wastes for Carbon Mineralization and Utilization Toward a Circular Economy. ACS Sustainable Chemistry and Engineering 5: 6429-6437.

Stokes Debbie, 2008. Principles and Practice of Variable Pressure/Environmental Scanning Electron Microscopy (VP-ESEM). John Wiley and Sons. ISBN 978-0470758748.

Vallero Daniel, 2014. Air Pollutant Emissions. Fundamentals of Air Pollution 5: 787-827.

Vautard Robert, Gobiet Andreas, Sobolowski Stefan, Kjellström Erik, Stegehuis Annemiek, Watkiss Paul, Mendlik Thomas, Landgren Oskar, Nikulin Grigory, Teichmann Claas and Jacob Daniela, 2014. The European climate under a 2 °C global warming. Environmental Research Letters 9 (3).

Wang George, Wang Yuhong and Gao Zhili, 2010. Use of steel slag as a granular material: Volume expansion prediction and usability criteria. Journal of Hazardous Materials 184 (1-3): 555-560.

Watson Rob, 2017. Landfill Waste Costs Continued to Rise in 2016. Solid Waste Environmental Excellence Protocol. URL: [https://nrra.net/sweep/cost-to-landfill-waste-continues-to-rise-through-2016/]. Cited 3.4.2019.

World Steel Association, 2018. Press release: World crude steel output increases by 5.3% in 2017. URL: [https://www.worldsteel.org/media-centre/press-releases/2018/World-crude-steel-output-increases-by-5.3--in-2017.html]. Cited 6.2.2019.

Wu Qiong, You Ruirong, Clark Malcolm and Yu Yan, 2014. Pb(II) removal from aqueous solution by a low-cost adsorbent dry desulfurization slag. Applied Surface Science 314: 129-137.

APPENDICES

27/5/2019 12.53.05
PANalytical
Quantification of sample De-S Markus Honkanen

R.M.S.:	0,004
Result status:	LoE;
Sum:	99,10 %
Sample type:	Fused bead
Initial sample weight (g):	0,5
Compton validation factor:	1,09
Oxygen validation factor:	1,12
Correction applied for medium:	No
Correction applied for film:	No
Used Compound list:	Oxides
Results database:	omnian
Results database in:	c:\panalytical\superq\userdata

Analyte	Calibration status	Compound formula	Concentration	Unit	Calculation method	Status
Na	Calibrated	Na2O	1,454	%	Calculate	BgC;DC;NFL;LoE;
Mg	Calibrated	MgO	1,645	%	Calculate	BgC;DC;
Al	Calibrated	Al2O3	2,154	%	Calculate	BgC;DC;
Si	Calibrated	SiO2	15,194	%	Calculate	BgC;DC;LoR;
P	Calibrated	P2O5	0,148	%	Calculate	BgC;DC;
S	Calibrated	SO3	4,987	%	Calculate	BgC;DC;LoR;
Cl	Calibrated	Cl	0,115	%	Calculate	BgC;DC;
K	Calibrated	K2O	0,214	%	Calculate	BgC;DC;
Ca	Calibrated	CaO	55,4	%	Calculate	BgC;DC;
Ti	Calibrated	TiO2	0,663	%	Calculate	BgC;DC;LoR;
V	Calibrated	V2O5	0,439	%	Calculate	BgC;DC;
Cr	Calibrated	Cr2O3	0,04	%	Calculate	BgC;DC;LoR;
Mn	Calibrated	MnO	0,488	%	Calculate	BgC;DC;
Fe	Calibrated	Fe2O3	16,061	%	Calculate	BgC;DC;LoR;
Ni	Calibrated	NiO	0,029	%	Calculate	BgC;DC;
Cu	Calibrated	CuO	0,031	%	Calculate	BgC;DC;
Zn	Calibrated	ZnO	0,009	%	Calculate	BgC;DC;
Sr	Calibrated	SrO	0,033	%	Calculate	BgC;DC;
Zr	Calibrated	ZrO2	0,009	%	Calculate	BgC;DC;LoR;
Nb	Calibrated	Nb2O5	0,011	%	Calculate	BgC;DC;

Sample treatment:
TGA 525°C LOI 8.0% 950°C LOI 15.0%
Planetary ball mill: 300rpm/2min
Fused bead 1200°C
Result treatment:
Au, Co removed

27/5/2019 12.53.20
PANalytical
Quantification of sample De-S Markus Honkanen

R.M.S.:	0,004
Result status:	LoE;
Sum:	99,10 %
Sample type:	Fused bead
Initial sample weight (g):	0,5
Compton validation factor:	1,09
Oxygen validation factor:	1,12
Correction applied for medium:	No
Correction applied for film:	No
Used Compound list:	Oxides
Results database:	omnian
Results database in:	c:\panalytical\superq\userdata

	Element	Conc. (%)
1	O	34,48
2	Na	1,079
3	Mg	0,992
4	Al	1,14
5	Si	7,102
6	P	0,06444
7	S	1,997
8	Cl	0,1151
9	K	0,1775
10	Ca	39,59
11	Ti	0,3972
12	V	0,2457
13	Cr	0,02729
14	Mn	0,3778
15	Fe	11,23
16	Ni	0,02267
17	Cu	0,02508
18	Zn	0,007016
19	Sr	0,02772
20	Zr	0,006984
21	Nb	0,007836

Flux

Chemical formula	Weight (g)
Li147B224O410	8,5
NH4I	0,02

Appendix 1. XRF result for desulfurization slag.

27/5/2019 12.52.05
PANalytical
Quantification of sample BOF Markus Honkanen

R.M.S.:	0,007
Result status:	
Sum:	100,30 %
Sample type:	Fused bead
Initial sample weight (g):	0,5
Compton validation factor:	1,09
Oxygen validation factor:	1,14
Correction applied for medium:	No
Correction applied for film:	No
Used Compound list:	Oxides
Results database:	omnian
Results database in:	c:\panalytical\superq\userdata

Analyte	Calibration status	Compound formula	Concentration	Unit	Calculation method	Status
Na	Calibrated	Na2O	0,113	%	Calculate	BgC;DC;
Mg	Calibrated	MgO	1,906	%	Calculate	BgC;DC;
Al	Calibrated	Al2O3	1,696	%	Calculate	BgC;DC;
Si	Calibrated	SiO2	14,326	%	Calculate	BgC;DC;
P	Calibrated	P2O5	0,985	%	Calculate	BgC;DC;
S	Calibrated	SO3	0,186	%	Calculate	BgC;DC;LoR;
K	Calibrated	K2O	0,143	%	Calculate	BgC;DC;
Ca	Calibrated	CaO	50,088	%	Calculate	BgC;DC;
Ti	Calibrated	TiO2	0,868	%	Calculate	BgC;DC;
V	Calibrated	V2O5	3,203	%	Calculate	BgC;DC;
Cr	Calibrated	Cr2O3	0,308	%	Calculate	BgC;DC;LoR;
Mn	Calibrated	MnO	2,864	%	Calculate	BgC;DC;LoR;
Fe	Calibrated	Fe2O3	23,362	%	Calculate	BgC;DC;LoR;
Ni	Calibrated	NiO	0,021	%	Calculate	BgC;DC;
Cu	Calibrated	CuO	0,024	%	Calculate	BgC;DC;
Sr	Calibrated	SrO	0,034	%	Calculate	BgC;DC;
Nb	Calibrated	Nb2O5	0,081	%	Calculate	BgC;DC;
Cl	Calibrated	Cl	0,12	%	Calculate	BgC;DC;

Sample treatment:
TGA 525°C LOI 3,1% 950°C LOI 9.9%
Planetary ball mill: 300rpm/2min
Fused bead 1200°C
Result treatment:
Au, W,Co, Th removed

27/5/2019 12.52.23
PANalytical
Quantification of sample BOF Markus Honkanen

R.M.S.:	0,007
Result status:	
Sum:	100,30 %
Sample type:	Fused bead
Initial sample weight (g):	0,5
Compton validation factor:	1,09
Oxygen validation factor:	1,14
Correction applied for medium:	No
Correction applied for film:	No
Used Compound list:	Oxides
Results database:	omnian
Results database in:	c:\panalytical\superq\userdata

	Element	Conc. (%)
1	O	33,75
2	Na	0,08375
3	Mg	1,149
4	Al	0,8974
5	Si	6,696
6	P	0,4299
7	S	0,07431
8	Cl	0,1204
9	K	0,1186
10	Ca	35,8
11	Ti	0,5201
12	V	1,794
13	Cr	0,2107
14	Mn	2,218
15	Fe	16,34
16	Ni	0,01627
17	Cu	0,01943
18	Sr	0,02881
19	Nb	0,0565

Flux

Chemical formula	Weight (g)
Li147B224O410	8,5
NH4I	0,02

Appendix 2. XRF result for non-carbonated BOF slag.

Sieve Size	Sample Mass	Percentage of Sample	Sample Mass	Percentage of Sample
	Desulfurization Slag		BOF Slag	
20 µm	4.4 g	7.3%	0.8 g	1.3%
32 µm	3.0 g	5.0%	0.3 g	0.5%
63 µm	5.0 g	8.3%	2.6 g	4.0%
125 µm	7.1 g	11.8%	2.6 g	4.0%
250 µm	10.9 g	18.2%	15.4 g	23.7%
500 µm	14.8 g	24.7%	15.2 g	23.4%
1000 µm	13.4 g	22.3%	10.1 g	15.5%
2000 µm	1.4 g	2.3%	10.2 g	15.7%
>2000 µm	0.0 g	0.0%	7.8 g	11.9%

Appendix 3. Particle size distribution of slag samples.

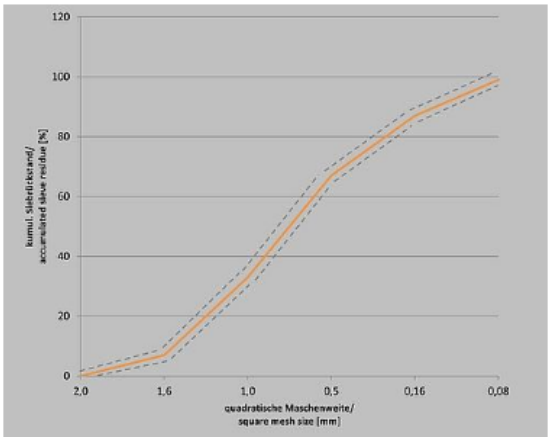

Mesh size (mm)	Lower limit	Intervall average	Upper limit
2,00	0	0	0
1,60	2	7	12
1,00	28	33	38
0,50	62	67	72
0,16	82	87	92
0,08	98	99	100

Appendix 4. Grain size distribution for CEN-Normsand DIN EN 196-1.

Aggregate to binder percentage / Curing time	Compressive strength	Aggregate to binder percentage / Curing time	Compressive strength
0%/60 min	12.26 MPa	**0%/120 min**	15.37 MPa
	14.68 MPa		12.10 MPa
	14.01 MPa		14.29 MPa
	12.38 MPa		16.01 MPa
25%/60 min	22.43 MPa	**25%/120 min**	15.48 MPa
	20.99 MPa		16.21 MPa
	20.92 MPa		15.46 MPa
	24.10 MPa		16.22 MPa
50%/60 min	8.56 MPa	**50%/120 min**	17.26 MPa
	12.20 MPa		15.72 MPa
	13.85 MPa		13.31 MPa
	13.40 MPa		14.91 MPa
100%/60 min	13.16 MPa	**100%/120 min**	13.25 MPa
	14.03 MPa		13.71 MPa
	12.22 MPa		
	13.01 MPa		
	13.29 MPa		
200%/60 min	6.35 MPa	**200%/120 min**	7.31 MPa
	7.58 MPa		7.68 MPa
	7.72 MPa		

Appendix 5. The compressive strengths of the initial samples.

Curing Time	Compressive Strength
15 min	10.67 MPa
	11.83 MPa
30 min	10.73 MPa
	10.34 MPa
60 min	10.39 MPa
	10.29 MPa
120 min	14.09 MPa
	12.04 MPa

Appendix 6. Compressive strengths of the De-S samples with different curing times.

Aggregate to binder percentage	Compressive strength
0%	1.73 MPa
	2.03 MPa
25%	2.37 MPa
	2.79 MPa
50%	1.67 MPa
100%	0.77 MPa
200%	0.65 MPa
	0.71 MPa

Appendix 7. Strength test results for non-carbonated De-S samples.

	Compressive strength with carbon sequestration	Compressive strength without carbon sequestration
BOF	1.93 MPa	unable to measure
	1.88 MPa	unable to measure
Pre-carbonated BOF	2.96 MPa	0.35 MPa
	2.25 MPa	0.18 MPa

Appendix 8. Compressive strengths of BOF samples.